HHS Public Access

Author manuscript

Nat Med. Author manuscript; available in PMC 2020 May 29.

Published in final edited form as:

Nat Med. 2019 November ; 25(11): 1739–1747. doi:10.1038/s41591-019-0610-4.

Adipsin preserves beta cells in diabetic mice and associates with protection from type 2 diabetes in humans

Nicolás Gómez-Banoy[1], **J. Sawalla Guseh**[2], **Ge Li**[3], **Alfonso Rubio-Navarro**[1], **Tong Chen**[1], **BreAnne Poirier**[1], **Gregory Putzel**[4], **Carolina Rosselot**[5], **Maria A. Pabón**[1], **João Paulo Camporez**[6], **Vijeta Bhambhani**[2], **Shih-Jen Hwang**[7,8], **Chen Yao**[7,8], **Rachel J. Perry**[6], **Sushmita Mukherjee**[3], **Martin G. Larson**[8,9], **Daniel Levy**[7,8], **Lukas E. Dow**[10], **Gerald I. Shulman**[6], **Noah Dephoure**[10], **Adolfo Garcia-Ocana**[5], **Mingming Hao**[3], **Bruce M. Spiegelman**[11], **Jennifer E. Ho**[2,*], **James C. Lo**[1,*]

[1]Weill Center for Metabolic Health and Division of Cardiology, Department of Medicine, Weill Cornell Medicine, New York, NY, USA.

[2]Corrigan Minehan Heart Center, Cardiovascular Research Center and Division of Cardiology, Department of Medicine, Massachusetts General Hospital, Harvard Medical School, Boston, MA, USA.

[3]Department of Biochemistry, Weill Cornell Medicine, New York, NY, USA.

[4]Jill Roberts Institute for Research in Inflammatory Bowel Disease, Department of Medicine, Weill Cornell Medicine, New York, NY, USA.

[5]Diabetes, Obesity and Metabolism Institute, Icahn School of Medicine at Mount Sinai, New York, NY, USA.

[6]Departments of Internal Medicine and Cellular & Molecular Physiology, Yale School of Medicine, New Haven, CT, USA.

[*]**Correspondence and requests for materials** should be addressed to J.E.H. or J.C.L., jho1@mgh.harvard.edu; jlo@med.cornell.edu.

Author contributions

J.C.L. and N.G.-B. designed the animal, cellular and molecular studies. J.E.H. and J.S.G. designed the human study. N.G.-B., G.L., A.R.-N., T.C., B.P., M.A.P., J.P.C. and R.J.P. performed and analyzed the animal experiments. N.G.-B, A.R.-N., T.C., B.P. and C.R. developed the in vitro experiments. J.E.H., J.S.G., V.B., S.-J.H., C.Y., D.L. and M.G.L. analyzed the human study data. S.M. analyzed microscope images. N.D. developed and analyzed proteomics experiments. G.P. analyzed RNA sequencing experiments. L.E.D., G.I.S., A.G.-O., M.H. and B.M.S. provided scientific input and analyzed the data. J.C.L., J.E.H., N.G.-B. and J.S.G. wrote the manuscript, and all authors contributed to writing and provided feedback. J.C.H. (jho1@mgh.harvard.edu) is the contact for the Framingham studies.

Online content

Any methods, additional references, Nature Research reporting summaries, source data, extended data, supplementary information, acknowledgements, peer review information; details of author contributions and competing interests; and statements of data and code availability are available at https://doi.org/10.1038/s41591–019-0610–4.

Competing interests

Cornell University has filed a provisional patent application that covers the use of DUSP26 inhibitors for the treatment of type 2 diabetes. (US patent application no. 62/740744; N.G.-B. and J.C.L.). V.B. is currently an employee of Fractyl Laboratories Inc. and all analyses were conducted during employment at Massachusetts General Hospital.

Extended data is available for this paper at https://doi.org/10.1038/s41591–019-0610–4.

Supplementary information is available for this paper at https://doi.org/10.1038/s41591–019-0610–4.

Peer review information Joao Monteiro was the primary editor on this article and managed its editorial process and peer review in collaboration with the rest of the editorial team.

[7]Population Sciences Branch, Division of Intramural Research, National Heart, Lung, and Blood Institute, National Institutes of Health, Bethesda, MD, USA.

[8]Framingham Heart Study, Framingham, MA, USA.

[9]Department of Biostatistics, Boston University School of Public Health, Boston, MA, USA.

[10]Sandra and Edward Meyer Cancer Center, Department of Medicine, Weill Cornell Medicine, New York, NY, USA.

[11]Dana-Farber Cancer Institute and Harvard Medical School, Boston, MA, USA.

Abstract

Type 2 diabetes is characterized by insulin resistance and a gradual loss of pancreatic beta cell mass and function[1,2]. Currently, there are no therapies proven to prevent beta cell loss and some, namely insulin secretagogues, have been linked to accelerated beta cell failure, thereby limiting their use in type 2 diabetes[3,4]. The adipokine adipsin/complement factor D controls the alternative complement pathway and generation of complement component C3a, which acts to augment beta cell insulin secretion[5]. In contrast to other insulin secretagogues, we show that chronic replenishment of adipsin in diabetic *db*/*db* mice ameliorates hyperglycemia and increases insulin levels while preserving beta cells by blocking dedifferentiation and death. Mechanistically, we find that adipsin/C3a decreases the phosphatase *Dusp26*; forced expression of *Dusp26* in beta cells decreases expression of core beta cell identity genes and sensitizes to cell death. In contrast, pharmacological inhibition of DUSP26 improves hyperglycemia in diabetic mice and protects human islet cells from cell death. Pertaining to human health, we show that higher concentrations of circulating adipsin are associated with a significantly lower risk of developing future diabetes among middle-aged adults after adjusting for body mass index (BMI). Collectively, these data suggest that adipsin/C3a and DUSP26-directed therapies may represent a novel approach to achieve beta cell health to treat and prevent type 2 diabetes.

Most treatments for type 2 diabetes (T2D) target insulin resistance or promote insulin secretion from beta cells, but none have been shown to prevent beta cell failure[6,7]. T2D patients with beta cell failure require insulin injections to maintain euglycemia and become ‘insulin dependent’[6,8,9].

Adipokines are secreted proteins from adipocytes that play a central role in metabolism[10]. Adipsin/complement factor D was the first described adipokine. It maintains adipose tissue homeostasis and increases insulin secretion in response to glucose[5]. Adipsin controls the alternative complement pathway to catalyze the production of C3a (an active form of complement component 3, C3), an insulin secretagogue[5]. However, it is unknown if chronic adipsin treatment would be a durable antihyperglycemic or lead to premature beta cell failure.

To assess the effect of adipsin on long-term beta cell maintenance, we transplanted pancreatic islets into the anterior chamber of the eyes of mice and tracked these reporter islets in real time[11,12]. *db*/*db* mice represent a model of T2D with obesity that develops beta cell failure, characterized by reduced beta cell mass, marked hypoinsulinemia, severe

hyperglycemia and adipsin deficiency[13,14]. Pancreatic islets from donor *db*/*db* mice were transplanted into recipient *db*/*db* mice, which were then treated with adeno-associated virus (AAV) expressing adipsin (*db*/*db*-Adipsin) or control GFP (*db*/*db*-GFP)[15]. Additionally, to assess the effect of adipsin overexpression in a non-diabetic model, wild-type (WT) mice were transplanted with WT islets and treated with AAV-Adipsin (WT-Adipsin) or AAV-GFP (WT-GFP). Importantly, *db*/*db*-Adipsin mice showed improvements in hyperglycemia (nearly reaching WT glucose levels by 4 months) and increased fasting insulin levels at 2–3 months post-treatment with an overall trend up to 5 months compared to *db*/*db*-GFP mice (Fig. 1a,b). Reporter islets in three out of five *db*/*db*-GFP mice showed progressive decline in islet area starting at 2 months, whereas adipsin-treated diabetic mice uniformly showed no signs of ocular islet atrophy (Fig. 1c,d). Moreover, transplanted islets in all the *db*/*db*-Adipsin mice showed a gradual increase in ocular islet area to more than 150% of the initial size (Fig. 1c,d). Notably, the *db*/*db*-GFP mice that had progressive ocular islet atrophy showed accompanying features of pancreatic beta cell failure such as marked hyperglycemia, insulinopenia, altered islet microarchitecture and dramatically reduced pancreatic beta cell area (Fig. 1e and Extended Data Fig. 1a–d). Our results demonstrate that the reporter islets in the eye reflect events transpiring within the pancreatic islets. Finally, no differences in fasting glucose, insulin, ocular islet morphology and growth were noted between WT-Adipsin and WT-GFP mice, suggesting that pharmacologically raising adipsin levels may be safe (Fig. 1a,b and Extended Data Fig. 1e–g). Together, these findings establish that overexpression of adipsin can successfully restrict pancreatic islet atrophy and conserve beta cells in a mouse model of T2D with beta cell failure.

AAV-Adipsin robustly sustained adipsin expression for the duration of the experiment (6 months) after a single injection of AAV (Fig. 1f and Extended Data Fig. 2a,b). Replenishment of adipsin resulted in almost double the amount of cleavage of total serum C3 into its active form C3a, suggesting AAV-Adipsin was catalytically active (Fig. 1g,h). Adipsin treatment consistently resulted in reduced fasting glucose and increased fasting insulin levels from 1.5 to 6 months post-transduction (Fig. 1i), without affecting body weight (Extended Data Fig. 2c). We performed hyperinsulinemic euglycemic clamps and observed no differences in glucose infusion rates, whole-body glucose uptake and endogenous glucose production (Fig. 1j,k and Extended Data Fig. 2d) between control and adipsin groups, indicating that adipsin had no significant effect on insulin sensitivity. Taken together, these results suggest that chronic adipsin replenishment ameliorates hyperglycemia predominantly by enhancing insulin levels.

Strikingly, *db*/*db*-Adipsin mice showed 35% higher beta cell mass at 1.5 months post-transduction (early diabetes) and nearly double that of controls at 6 months post-transduction (late diabetes) (Fig. 2a,b). The difference in beta cell mass at 6 months was driven by ~40% of mice in the control group that developed severely diminished beta cell mass and distorted islet architecture (Fig. 2a–c). Importantly, these control mice developed bona fide beta cell failure, defined as low beta cell mass (<3 mg), severe hyperglycemia (>450 mg dl^{-1}) and profound insulinopenia (<3 ng ml^{-1}) (Extended Data Fig. 2e–g). Remarkably, none of the mice receiving AAV-Adipsin developed beta cell failure (Fig. 2c).

To discern how adipsin might lead to sustained preservation of beta cell mass, we assayed for changes in beta cell death and proliferation. At 1.5 months post-AAV, there was no significant difference in beta cell death between the groups (Fig. 2d,e and Extended Data Fig. 3a,b). By contrast, at 6 months post-transduction when more beta cells show signs of cell death, adipsin robustly decreased the number of $TUNEL^+$ and cleaved caspase 3 $(CC3)^+$ beta cells by three- to fourfold compared to GFP, indicating protection from cell death (Fig. 2d,e and Extended Data Fig. 3a,b). We found no difference between the groups in beta cell proliferation as ascertained by Ki67 staining (Extended Data Fig. 3c,d) or 5-bromo-2′-deoxyuridine (BrdU) labeling (Fig. 2f,g). Taken together, our results indicate that adipsin does not affect beta cell proliferation but conserves beta cell mass by inhibiting beta cell death.

Alterations in the alpha-to-beta cell ratio within the pancreatic islet and hyperglucagonemia may also contribute to the pathogenesis of T2D[16–18]. We found decreased alpha cell mass at 1.5 months and a similar trend at 6 months post-transduction in the *db*/*db*-Adipsin mice compared to controls (Extended Data Fig. 3e,f). Critically, the alpha-to-beta cell ratio was maintained at WT levels at 6 months in adipsin-treated mice, whereas control mice had an elevated alpha-to-beta cell ratio without changes in serum glucagon levels (Extended Data Fig. 3g,h). This raised the possibility that the higher alpha-to-beta cell ratio in the *db*/*db*-GFP mice may be due to beta cell dedifferentiation and that adipsin might promote beta cell maintenance[19]. We found a significant presence of Ins^+Gcg^+ cells in the islets of *db*/*db*-GFP mice compared to virtually none in *db*/*db*-Adipsin mice, suggesting upregulation of non-beta cell programs in control mice (Fig. 2h). Previous work has shown that beta cells lose key beta cell transcription factors in the context of T2D[20]. To investigate whether adipsin has an effect on the maintenance of beta cell transcriptional identity, we performed immunostaining for MAFA, NKX6.1 and NKX2.2. *db*/*db*-Adipsin mice exhibited increased numbers of beta cells positive for MAFA (Extended Data Fig. 4a,b), NKX6.1 (Fig. 2i) and NKX2.2 (Extended Data Fig. 4c,d) compared to controls. We also performed immunostaining for aldehyde dehydrogenase 1a3 (ALDH1A3) and gastrin, which are molecular markers of failing or dedifferentiated beta cells[21,22]. Adipsin treatment decreased the number of $ALDH1A3^{hi}$ beta cells (Fig. 2j) and virtually eliminated the presence of $gastrin^+$ cells (Extended Data Fig. 4e,f). Our results suggest that adipsin protects against beta cell failure by maintaining beta cell transcriptional identity and blocking dedifferentiation. We have previously shown that adipsin increases the generation of C3a, which acts on the pancreatic islets to promote insulin secretion[5]. We now demonstrate that C3a can act directly on INS-1 beta cells to induce insulin secretion (Extended Data Fig. 5a). Furthermore, we tested whether C3a could protect beta cells from death. We subjected INS-1 cells and pancreatic islets to palmitate (lipotoxicity) and cytokine toxicity. Remarkably, C3a treatment reduced caspase-3 activation to half in INS-1 cells (Fig. 3a,b) and reduced the expression of cell death markers in pancreatic islets (Fig. 3c and Extended Data Fig. 5b). To elucidate the molecular mechanisms behind the protective effects of C3a on beta cells, we performed RNA–seq analyses on isolated WT islets cultured in vehicle and palmitate conditions with or without recombinant C3a. We found a subset of genes that were significantly altered by palmitate and further counter-regulated by C3a (Extended Data Fig. 5c). Interestingly, unbiased gene ontology (GO) molecular function analysis on the set of genes whose

expression was downregulated by palmitate and counter-regulated (increased) by C3a revealed that positive regulation of glycolytic processes and coenzyme metabolic processes were the top associated pathways (Extended Data Fig. 5d). Previous reports have shown that palmitate interferes with glucose metabolism, calcium signaling and insulin secretion in beta cells, leading to cell dysfunction and death[23]. Furthermore, GO analysis on the set of genes whose expression was induced by palmitate and counter-regulated (decreased) by C3a showed negative regulation of calcium-dependent exocytosis as the top pathway, further suggesting that C3a may oppose palmitate's negative effect on insulin secretion (Extended Data Fig. 5e).

To further explore the molecular mechanisms behind the protective effects of adipsin/C3a, we isolated pancreatic islets from *db*/*db*-GFP and *db*/*db*-Adipsin mice and performed unbiased transcriptomic profiling at 1 month post-transduction, when serum glucose levels were similar between both groups. RNA–seq analyses revealed six genes that were significantly changed by adipsin. The only gene whose expression was downregulated was dual specificity protein phosphatase 26 (*Dusp26*; Fig. 3d). Interestingly, our pathway analysis of C3a-treated islets showed that C3a regulates the expression of protein substrates of DUSP26 (Extended Data Fig. 5f). Additionally, we found that C3a downregulated *Dusp26* expression in beta cells. Interestingly, palmitate increased the expression of *Dusp26*, while C3a counter-regulated *Dusp26* in this lipotoxic condition (Fig. 3e).

To determine if DUSP26 plays a role in beta cell homeostasis, we performed gain and loss of function experiments with DUSP26 in beta cells and pancreatic islets. Forced expression of *Dusp26* resulted in a significant decrement in the expression of core beta cell genes such as *Ins2*, *Mafa*, *Nkx6.1* and *Nkx2.2* (Fig. 3f). Similarly, forced expression of *Dusp*26 in islet cells decreased the expression of *Ins2* and increased the expression of *Gcg* (Extended Data Fig. 5g). Remarkably, beta cells overexpressing *Dusp26* showed double the amount of CC3 (Fig. 3g,h) and exhibited decreased cell viability when exposed to palmitate (Extended Data Fig. 5h) compared to controls. In stark contrast, knockdown of *Dusp26* (Extended Data Fig. 5i,j) significantly increased the expression of key beta cell factors such as *Ins2*, *Mafa*, *Nkx6–1* and *Nkx2–2* (Fig. 3i) and halved caspase-3 activation in response to palmitate (Fig. 3j,k).

DUSP26 expression is enriched in neuroendocrine tissues[24]. We explored the possibility that DUSP26 phosphatase activity may contribute to beta cell failure by using NSC-87877, a pharmacological inhibitor of this phosphatase in beta cells[25,26]. Notably, NSC-87877 partially reversed the effects of palmitate, increasing cell viability (Fig. 3l). To investigate a potential role for pharmacological inhibition of DUSP26 in vivo, we treated *db*/*db* mice with NSC-87877 (Extended Data Fig. 5k). Remarkably, mice receiving NSC-87877 exhibited decreased glycemia compared to saline-treated controls, which exhibited worsening hyperglycemia relative to baseline (Fig. 3m). In support of DUSP26 inhibition improving beta cell function, circulating insulin levels were dramatically reduced in control mice, whereas this reduction was attenuated in NSC-87877-treated mice (Fig. 3n). To assess if antagonism of DUSP26 can block beta cell failure, we performed ALDH1A3 staining and found that NSC-87877 reduced ALDH1A3^{hi} cells by 80% compared to controls (Fig. 3o,p). To test whether DUSP26 inhibition could translate to improved beta cell outcomes in humans, we treated human islets with NSC-87877. Importantly, NSC-87877 completely

protected against palmitate-induced beta cell death in human islets (Fig. 4a,b). To explore the potential substrates and factors associated with DUSP26 in beta cells, we purified DUSP26 from INS-1 cells overexpressing DUSP26 and a catalytically inactive DUSP26 (C152S) mutant as a substrate trap and performed proteomic analyses (Extended Data Fig. 5l). Mass spectrometry analysis of the DUSP26-interacting proteins showed enrichment of proteins involved in metabolic and cell death pathways, suggesting a possible mechanism by which DUSP26 regulates beta cell function and survival (Extended Data Fig. 5m,n). Future work will be needed to more broadly define and functionally assess the DUSP26 interactome and substrates that contribute to beta cell homeostasis. Our genetic gain and loss of function studies show that Dusp26 promotes cell death and decreases the expression of core beta cell identity genes. A previous study, by contrast, showed that miR-200 regulates *Dusp26* in beta cells and silencing *Dusp26* reduced beta cell viability, potentially through a mechanism involving p53 phosphorylation[27]. We present further supporting evidence for a deleterious role of Dusp26 in beta cells, as pharmacological manipulation of this enzyme with a chemical inhibitor protected beta cells from lipotoxicity and led to improved beta cell function in diabetic mice and human islets. Our study provides a proof of concept that DUSP26 inhibition could serve as a pharmacological target for T2D.

Beta cell dysfunction is integral to the development of T2D[6,9,28]. We have previously shown that circulating adipsin is decreased in patients with T2D and beta cell failure compared to T2D patients without beta cell insufficiency[5]. A recent clinical study also found that newly diagnosed T2D patients had lower levels of adipsin compared to non-diabetic individuals[29]. However, the relationship between adipsin and the development of T2D is not clear, as longitudinal studies examining a potential association have not been performed. Here, we assessed circulating plasma adipsin concentrations from 6,886 participants in the Framingham Heart Study (Extended Data Fig. 6).

In cross-sectional multivariable analyses, higher adipsin concentrations were independently associated with lower odds of diabetes mellitus and greater odds of obesity (Extended Data Fig. 7). Specifically, a 1 s.d. increase in adipsin was associated with a more than 30% decreased odds of diabetes after accounting for BMI (odds ratio (OR) 0.67, 95% confidence intervals (CI) 0.61–0.78, $P < 0.0001$). Conversely, a 1 s.d. increase in adipsin was associated with a 68% increased odds of obesity. When examining continuous clinical traits, higher adipsin levels were significantly associated with higher BMI and inversely associated with fasting glucose (Extended Data Fig. 7).

Visceral adiposity is associated with increased cardiometabolic risk[30]. Therefore, we sought to characterize the type of adiposity associated with adipsin. Adipsin was associated with subcutaneous and intrathoracic adipose volumes but not visceral adiposity (Extended Data Fig. 7).

Notably, when participants were followed longitudinally for the development of incident diabetes, we found that higher baseline adipsin concentrations were associated with a lower risk of future diabetes. Specifically, a 1 s.d. increase in adipsin was independently associated with 29% decreased odds of future diabetes in multivariable adjusted analyses (Fig. 4c). In secondary analyses, we additionally accounted for adipose depots (visceral and

subcutaneous) and found that adipsin remained associated with a lower risk of future diabetes (OR = 0.69, 95% CI = 0.53–0.78, $P < 0.0001$). Individuals with adipsin concentrations in the highest quartile had over 50% reduction in odds of diabetes when compared with the lowest quartile (Fig. 4d). Given that obesity predisposes to diabetes and is associated with adipsin concentrations in our study, we found that BMI modified the association of adipsin with future diabetes ($P = 0.027$ for interaction). In stratified analyses comparing obese and non-obese individuals, greater adipsin concentrations were associated with 34% decreased risk of future diabetes risk among obese individuals (multivariable-adjusted OR = 0.66, 95% CI = 0.53–0.81, $P < 0.0001$), whereas this association was attenuated among non-obese individuals (OR = 0.79, 95% CI = 0.61–1.02, $P = 0.07$) (Fig. 4e).

Given the observed association between elevated adipsin levels and decreased T2D risk, we explored potential genetic regulators of adipsin expression through a GWAS and found four independent *cis* variants that were associated with circulating adipsin concentrations (Fig. 4f and Extended Data Fig. 8a,b). The strongest association for adipsin was found on chromosome 19p13.3 (lead SNP rs2930902, $P = 1.36 \times 10^{-7}$) (Extended Data Fig. 8a,b). Open source queries of all four *cis* variants revealed strong associations with T2D (Extended Data Fig. 9)[31–34]. We queried rs2930902 against known expression quantitative trait loci (eQTL) databases and found significant *cis*-eQTL associations with tissue-specific upregulation of *ADIPSIN* in several tissues, including subcutaneous adipose ($P = 0.0026$). We found associations between rs2930902 and the metabolites valine and glycine, each of which has been shown to inform incident human diabetes risk[35,36] (Extended Data Fig. 9).

Although some approaches show promise, there are currently no proven clinical therapies that can restore or maintain beta cell function and numbers for patients with T2D once beta cell failure has ensued[6]. Our study shows that restoration of adipsin in diabetic mice not only improves hyperglycemia, but also preserves beta cell mass by enhancing beta cell survival and maintaining beta cell transcriptional identity. This sets adipsin apart as a potential therapeutic target, as existing therapies such as insulin and thiazolidinedione (TZD) lower glycemia in *db*/*db* mice without affecting molecular markers of beta cell dedifferentiation[37]. The protective effect of adipsin in our experimental studies is further bolstered by the observation that higher adipsin portends a lower risk of future diabetes in middle-aged adults, particularly among obese individuals. We also found that higher concentrations of circulating adipsin were associated with subcutaneous but not visceral adipose depots. Adipsin, therefore, may serve as a biomarker of favorable adipose function and distinguish metabolic health from disease among the obese. Here we show that a single baseline adipsin measurement is independently associated with a lower risk of future diabetes at a given level of BMI. It is possible that adipsin levels may continue to decline in at risk individuals. Ideally, future studies will incorporate serial measures of adipsin within a given individual to capture the integrated exposure of adipsin over time on longitudinal diabetes risk. Mild to moderate decreases in adipsin levels over years of metabolic stress in humans may ultimately trigger beta cell dysfunction and diabetes. Comparatively, mice have higher circulating adipsin than humans. Mouse adipsin is glycosylated and more stable in the circulation, which could explain the difference between mouse and humans. Assays for adipsin activity may be informative. Moreover, our mechanistic studies show that adipsin is

functional, suggesting that replenishment of adipsin in T2D patients may be therapeutic. However, we cannot exclude the possibility that some of the beneficial effects of adipsin are independent of C3a/C3a receptor 1 (C3aR1). Further studies targeting C3a or C3aR1, specifically in beta cells, are needed. It remains an open question as to how adipsin is regulated in human diseases and how the alternative complement pathway evolved to regulate beta cell function. From a therapeutic perspective, we identify DUSP26 as a critical phosphatase downstream of adipsin/C3a that regulates beta cell survival and identity. We provide a proof of concept that pharmacological inhibition of DUSP26 may represent a novel therapeutic target for T2D. NSC-87877, however, can inhibit other phosphatases, although with lower potencies[26]. Thus, more selective and potent DUSP26 inhibitors need to be developed. Future studies to identify DUSP26 substrates relevant to beta cell biology in T2D are warranted.

In conclusion, our study demonstrates adipsin to be protective in T2D via unique effects on beta cell health. We show that adipsin may exert beneficial effects via C3a and lowering DUSP26, which may be leveraged into new pharmacotherapies to overcome beta cell failure in T2D.

Methods

Experimental animals.

B6.BKS(D)-Leprdb/J (*db*/*db*) homozygous mice were purchased from Jackson Laboratories. C57BL/6 WT mice used for islet isolation experiments were purchased from Jackson Laboratories. All mice were housed in plastic cages on a 12 h/12 h light/dark cycle with free access to water and food. All animal work was approved by the Institutional Animal Care and Use Committee and Research Animal Resource Center at Weill Cornell Medical College.

Islet transplantation and in vivo imaging.

Islet transplantation and in vivo imaging have been described previously[12]. In brief, mouse islets from B6 WT and *db*/*db* mice were isolated the day before transplantation and cultured overnight in RPMI 1640 with 10% FBS. For the transplantation, *db*/*db* or B6 WT mice were first anesthetized with ketamine/xylazine. Under the microscope, a pore on the cornea was made using a 26 G needle. Through the pore, islets were perfused into the anterior chamber of the eye through a 26 G cannula. After 2 days of recovery, the mice were observed weekly or biweekly by light microscopy for changes in gross size and morphology.

AAV vector preparation and injection.

AAVs were purchased from the Vector Core, University of Pennsylvania. Murine adipsin cDNA was cloned into the AAV8 vector. For AAV overexpression studies, *db*/*db* mice were injected intravenously route at 6–10 weeks of age with GFP or adipsin-expressing AAV vectors. AAV dosage was 5×10^{10} genomic copies of AAV per mouse, delivered in 150 μl of saline. Systemic overexpression was routinely checked with serum adipsin western blots 2 weeks post viral injection.

Hyperinsulinemic–euglycemic clamps.

Hyperinsulinemic–euglycemic clamps were performed as previously described[38]. Jugular venous catheters were inserted 7 days before hyperinsulinemic–euglycemic clamps. To assess basal whole-body glucose turnover, [3-^{3}H]glucose (HPLC purified, Perkin-Elmer) was infused at a rate of 0.05 μCi min^{-1} for 120 min into the jugular catheter after overnight fasting. After the basal infusion, hyperinsulinemic–euglycemic clamps were performed in conscious mice for 140 min with a 3 min primed infusion of insulin (48 mU kg^{-1} min^{-1}), followed by a continuous (20 mU kg^{-1} min^{-1}) infusion of human insulin (Novolin, Novo Nordisk), a variable infusion of 20% dextrose to maintain euglycemia (100–120 mg dl^{-1}) and [3-^{3}H]glucose at a rate of 0.1 μCi min^{-1} to calculate whole-body glucose turnover during the clamps. At the end of the clamps, mice were anesthetized with pentobarbital sodium injection (150 mg kg^{-1}), tissues were rapidly excised and snap-frozen in liquid nitrogen, then stored at −80 °C for subsequent analysis.

Treatment with NSC-87877.

For treatment with NSC-87877 compound (Sigma, BOSCI), 10-week-old *db*/*db* mice were treated with intraperitoneal injections of NSC-87877 or saline solution (30 mg^{-1} kg^{-1}) daily for 2 weeks. Weight and fasting blood samples were obtained every week and at the time of euthansia.

BrdU labeling.

BrdU (Sigma) was injected intraperitoneally at 1 mg per mouse for five continuous days before mouse sacrifice. Detection of $BrdU^+$ beta cells in mouse pancreatic sections was performed with a rat monoclonal anti-BrdU antibody (Abcam).

Blood glucose measurements.

Mice were fasted for 6 h and fasting blood samples were taken from the tail vein and assayed with a glucometer (OneTouch).

Blood chemistry analysis.

For measuring mouse serum insulin levels, mice were fasted for 6 h and blood was collected from the tail vein, the serum was separated by centrifugation and insulin was measured by ELISA (Crystal Chem). For measuring glucagon levels, blood was collected from the tail vein into EDTA-treated collection tube with aprotinin. Plasma was separated by centrifugation. Glucagon concentrations were determined by ELISA (ALPCO). Serum adipsin levels were determined by ELISA (R&D) following the manufacturer's recommendations.

Antibodies and reagents.

The following antibodies were used in IHC and IF: guinea pig anti-insulin (DAKO, #A0564, 1:1,000), rabbit anti-glucagon (Phoenix, #H-028–05, 1:2,000), rabbit anti Ki67 (Abcam, #ab16667, 1:200), rabbit anti-cleaved caspase 3 (Cell Signaling, #9661, 1:200), rat anti-BrdU (Abcam, #ab6326, 1:200), mouse anti-Nkx6–1 (Hybridoma Bank, #F55A12, 1:100) rabbit anti-Mafa (Bethyl, #IHC-00352, 1:100), rabbit anti-Nkx2–2 (Sigma, #HPA003468,

1:100), rabbit anti-ALDH1A3 (Novus, #NBP2–15339, 1:100) and rabbit anti-gastrin (Millipore, #256A, 1:200). The following antibodies were used for western blot: rabbit anti-cleaved caspase 3 (Cell Signaling, #9661, 1:1,000), rabbit anti-adipsin (Santa Cruz, #sc-50419, 1:1,000), chicken anti-C3a (Abcam, #ab48581, 1:1,000), rabbit anti-Dusp26 (Invitrogen, #PA5–22013, 1:1,000), rabbit anti-actin (Cell Signaling, #8456, 1:1,000) and mouse anti-FLAG (Sigma, #A8592, 1:1,000). Recombinant C3a (R&D) was used at a concentration of 100 nM. NSC-87877 compound was dissolved in PBS and used at 20 μM concentration.

Pancreatic islet isolation and culture.

Mouse pancreatic islets were isolated by perfusion of the pancreases with CiZyme (VitaCyte) through the common hepatic duct. Pancreases were removed and digested at 37 °C for 17 min. After two washes with RPMI medium with 3% FBS, islets were separated into a gradient using RPMI medium and Histopaque (Sigma-Aldrich). Islets were then hand-picked to avoid exocrine contamination and processed for different applications. For treatment with palmitate, recombinant C3a or NSC-87877, an equal number of whole handpicked islets were cultured in 11 mM glucose and 0.5 mM palmitate or vehicle and then harvested. For viral transduction of islets, dissociation was performed with 0.25% trypsin and cells were plated in 96-well formats.

Human islets and donors.

Human islets were obtained from Prodo Labs from two different healthy male donors (49 and 50 years old). Islet purity assessed by dithizone staining was 90% in both cases. Human islet cell cultures were prepared as previously published[39] and treated with 0.5 mM palmitate and 20 μM NSC-87877 in 11 mM glucose.

Western blot analysis.

Cells were homogenized in radioimmunoprecipitation assay (RIPA) buffer with protease inhibitor cocktail and phosphatase inhibitor cocktail. Protein extracts were resolved on a NuPAGE Bis-Tris (Thermo) gel and transferred to a PVDF membrane. Membranes were incubated overnight at 4 °C with appropriate primary antibodies. Detection of proteins was carried out by incubations with horseradish peroxidase (HRP)-conjugated secondary antibodies followed by enhanced chemiluminescence detection reagents. For serum western blots, protein from serum samples was denatured with NuPAGE (Thermo) reducing agent and then loaded onto a NuPAGE Bis-Tris (Thermo) gel. Band density was quantified using Fiji/ImageJ (NIH).

TUNEL and cell viability assays.

For determination of apoptosis in paraffin-embedded pancreatic sections and dispersed human islets, a TUNEL assay (Roche) was performed according to the manufacturer's instructions. $TUNEL^+$ nuclei surrounded by insulin-positive staining were determined with Fiji/ImageJ (NIH). For determination of cell viability, 50,000 INS-1 cells per well were seeded in a 24-well plate and subjected to specific treatments. Cell viability was determined

by measuring adenosine triphosphate (ATP) content using a CellTiter-Glo (Promega) kit according to the manufacturer's instructions.

IHC and IF analyses.

For histological studies of islets, pancreases were dissected, laid flat for paraffin embedding and fixed in 10% neutral-buffered formalin (VWR) overnight at 4 °C. Tissues were then transferred to 70% ethanol and subsequently embedded in paraffin and sectioned at 5 μm thickness. Sections were dewaxed, and antigen retrieval was performed using 10 mM sodium citrate buffer (pH 6.0) at boiling temperature for 14 min. Paraffin sections with the largest tissue surface area were used. For insulin and glucagon IHC to determine beta and alpha cell mass, anti-insulin and anti-glucagon antibodies were incubated overnight at 4 °C, followed by incubation with corresponding biotinylated secondary antibodies. HRP-conjugated avidin–biotin complex reagent was used following the manufacturer's protocol (Vector). Signals were developed using 3,3′-diaminobenzidine (DAB). Sections were then counterstained with hematoxylin. For IF staining, appropriate primary antibodies were incubated overnight at 4 °C, followed by incubation with Alexa-Fluor conjugated secondary antibodies (Thermo). For MAFA, NKX6.1 and NKX2.2 stainings, Tyramide Signal Amplification (TSA; Thermo) was used. HRP-conjugated secondary antisera were applied for 1 h at room temperature and posteriorly a Tyramide working solution was applied for 10 min at room temperature. Nuclei were counterstained with DAPI. To calculate beta and alpha cell mass, whole sections stained with insulin or glucagon and developed with DAB were scanned using a Leica SCN400 F whole-slide scanner. The fraction of insulin-positive or glucagon-positive areas compared to total pancreatic tissue area (hematoxylin) was determined with Fiji/ImageJ (NIH). Beta cell mass or alpha cell mass were then determined by multiplying the obtained fraction by the initial pancreatic wet weight. For IF analyses, images from pancreatic sections were obtained with a Nikon Eclipse Ti microscope or a Zeiss Axio Observer.Z1 confocal microscope at ×40 magnification. Insulin-positive cells were determined by counting the number of DAPI positive cells within the insulin staining area. Insulin-positive cells positive for beta cell transcription factors, Ki67, BrdU and TUNEL, were determined by counting the corresponding nuclear staining surrounding the insulin staining area. An arbitrary threshold for ALDH1A3^{hi} cells was determined and the number of DAPI-positive cells was established in areas where insulin and ALDH1A3 staining overlapped. Quantification of double-positive cells for insulin and glucagon was performed manually by two independent investigators using orthogonal projection images from *z* stacks obtained by confocal microscopy. For all analyses, at least 2,000 insulin-positive cells from 10–15 islets per animal were considered. All analysis and quantification were performed with Fiji/ImageJ (NIH).

Flow cytometry.

For flow cytometry, islets were dispersed into a single-cell suspension with trypsin/EDTA treatment. Staining was performed with a PE annexin V apoptosis detection kit (BD Pharmingen) and cells were analyzed on a FACSCanto II system (BD Biosciences).

Cell culture, viral transduction and palmitate treatment.

Rat INS-1 nano-Luc cells[40] were maintained in RPMI 1640 supplemented with 10% FBS, 10 mM HEPES, 2 mM l-glutamine, 1 mM sodium pyruvate and 0.05 mM 2-mercaptoethanol. 293T cells (to produce lentivirus) were grown in DMEM medium containing 4.5 g l^{-1} glucose, 10% FBS and 100 U ml^{-1} penicillin/streptomycin under a 5% CO_2 atmosphere at 37 °C. INS-1 cells were transduced at a 1:1 ratio with lentivirus containing pCDH or pRRL plasmids followed by puromycin selection. For induction of beta cell and islet apoptosis, sodium palmitate (Sigma) was dissolved to 150 mM in 50% ethanol at 60 °C, conjugated to 10% fatty acid-free BSA (Sigma) at 37 °C for 2 h and added to warm RPMI 1640 to a final concentration of 0.5 mM palmitate.

Insulin secretion assays.

INS-1 nano-Luc cells[40] were plated in 24-well plates at 70% confluency. The following day, cells were pre-incubated for 2 h in RPMI 1640 with no glucose, followed by 1 h in Krebs Ringer buffer (KRB) with 0 mM glucose. Cells were then stimulated for 30 min in fresh KRB containing varying amounts of glucose and recombinant C3a. Cell supernatant was assayed for luciferase activity using NanoLuc reagent (Promega).

Immunoprecipitation of DUSP26 and liquid chromatography with tandem mass spectrometry analysis.

Proteins interacting with DUSP26 were purified from cell lysates of INS-1 beta cells stably expressing FLAG-tagged DUSP26, FLAG-tagged DUSP26 C152S mutant or control GFP. Cells from 10 cm dishes were lysed in lysis buffer (50 mM Tris-HCl, pH 7.5, 150 mM NaCl, 0.5% NP-40) with protease inhibitor cocktail and 1 mM PMSF for 1 h with gentle rocking at 4 °C. Lysates were cleared using centrifugation (15,000 r.p.m., 20 min), and the supernatant was filtered through 0.45 μm pore-size spin filters to further remove cell debris and posteriorly pre-cleared with protein A/G magnetic beads (Thermo) for 1 h at 4 °C. Then, 300 μg of protein from the lysates was incubated with 60 μl of anti-FLAG M2 magnetic beads (Sigma) overnight at 4 °C. Beads with purified proteins were washed five times with 1 ml of ice-cold lysis buffer followed by three 1 ml PBS washes. Proteins were eluted by competition with 3× FLAG peptide (250 μg ml^{-1}) in a total volume of 150 μl in PBS.

Eluted immunocomplexes were precipitated with trichloroacetic acid (TCA, 20% wt/vol), rinsed three times with ice-cold acetone and dried at room temperature. The pellets were resuspended in 50 μl resuspension buffer (8 M urea, 50 mM ammonium bicarbonate and 5 mM DTT) and subjected to reduction and alkylation. Briefly, 15 mM chloroacetamide was added to each sample for 30 min in the dark at room temperature, followed by addition of another 5 mM DTT to quench the reaction. Samples were diluted to a final concentration of 2 M urea with 50 mM ambic and digested overnight at room temperature with 5 ng μl^{-1} LysC (Wako, #12–02541), then diluted to 1 M urea and digested for 6 h at 37 °C with trypsin (Promega, #V5111). Peptide digests were acidified by adding formic acid to 1% final concentration and desalted by solid-phase extraction on handmade C18 columns as previously described[41]. Desalted peptides were dried in a SpeedVac device then resuspended in 5% formic acid and analyzed by nanospray liquid chromatography with tandem mass spectrometry (LC-MS/MS) on an Orbitrap Fusion mass spectrometer (ThermoFisher).

Peptides were separated by reverse-phase HPLC on a hand-packed column (packed with 40 cm of 1.8 μm, 120 Å pores, Sepax GP-C18, Sepax Technologies) using a 75 min gradient of 5–23% buffer B (acetonitrile, 0.1% formic acid) at 350 nl min^{-1}. Peptides were detected using a Top 3 s method; for every survey scan, the instrument collects as many MS/MS scans as it can for up to 3 s and then proceeds with the next survey scan. For each cycle, one full MS scan of m/z = 3,750–1,400 was acquired in the Orbitrap at a resolution of 120,000 at m/z with an automatic gain control target = 5×10^5. Each full scan was followed by the selection of the most intense ions for CID and MS/MS analysis in the linear ion trap for 3 s. Selected ions were excluded from further analysis for 40 s. Ions with charge 1+ or unassigned were also rejected. Maximum ion accumulation times were 100 ms for each full MS scan and 35 ms for MS/MS scans.

MS2 spectra were searched using SEQUEST against a composite database containing all *Rattus norvegicus* proteins (36,107 total entries, downloaded from UniProt 5/14/19), common contaminants and the reversed decoy sequences of both using the following parameters: a precursor mass tolerance of ±20 ppm; 1.0 Da product ion mass tolerance; tryptic digestion; up to two missed cleavages; static modifications of carbamidomethylation on cysteine (+57.0214); dynamic modification of methionine oxidation (+15.9949). Peptide spectral matches were filtered to 1% false discovery rate (FDR) using the target–decoy strategy[42] combined with linear discriminant analysis (LDA) using SEQUEST scoring parameters including Xcorr, ΔCn′, precursor mass error and charge state[43].

Peptides were quantified based on the maximum signal-to-noise of their precursor ion intensity traces. Protein quantification was derived from the sum of these values for all peptides matching each protein. Technical replicates were combined for the analyses.

Pathway analysis.—Enrichr[44,45] was utilized for pathway analyses on proteins associated with DUSP26 in INS-1 beta cells.

Plasmids, shRNA and recombinant lentiviruses.

Mouse Dusp26 and the phosphatase-dead Dusp26 C152S expressing vectors were generated by PCR amplification of 630 bp fragments of the genomic sequences of Dusp26. Fragments were cloned at BamHI/EcoRI sites of the pCDH-FLAG backbone for lentivirus production. Constructs were confirmed by DNA sequencing. Posteriorly, pCDH-FLAG-Dusp26, pCDH-FLAG-Dusp26 C152S and control plasmids were transfected into 293T cells for production of lentivirus. For silencing of rat *Dusp26*, microRNA-based shRNAs were utilized. The shRNAs were designed using the SplashRNA algorithm[46]. A 97 bp cassette containing the micro-RNA-based shRNA was cloned into the pRRL.SFFV.GFP.mirE.PGK.Puro backbone. The antisense guide shRNA sequence was TTCAGTGAGAATATGACCACCT. The resulting plasmid was transfected into 293T cells along with appropriate cassettes to generate lentivirus expressing the shRNA. Lentivirus with an empty pRRL vector was used as control.

RNA extraction and qPCR analysis.

RNA isolation was performed using the RNeasy Micro and Mini kits (Qiagen). cDNA was synthetized through reverse transcription using a cDNA synthesis kit (Thermo). cDNA was analyzed by real-time PCR using specific gene primers and a SYBR Green Master Mix (Quanta). Primer sequences are shown in Supplementary Table 1.

Illumina RNA sequencing.

Library preparation and sequencing.—Following RNA isolation, total RNA integrity was checked using an Agilent 2100 Bioanalyzer. RNA concentrations were measured using the NanoDrop Spectrophotometer (Thermo Fisher Scientific). Preparation of the RNA sample library and sequencing were performed by the Genomics Core Laboratory at Weill Cornell Medicine. Messenger RNA was prepared using a TruSeq Stranded mRNA Sample Library Preparation kit (Illumina), according to the manufacturer's instructions. The normalized cDNA libraries were pooled and sequenced on an Illumina HiSeq4000 sequencer at 50 pair-end cycles.

Data analysis.—WT islets treated with palmitate and C3a. Transcript quantification was performed on the raw demultiplexed FASTQ files using Kallisto[47] against the Ensembl mouse transcriptome GRCm38 release 79, with 30 bootstrap samples and the options -bias (sequence-based bias correction) and -rf-stranded (strand specific reads, first read reverse). The resulting abundance estimates were imported into the DESeq2 R package[48] using the tximport R package[49] generating estimated normalized counts. Before differential expression analysis, transcripts with fewer than 100 total normalized counts across all samples were removed. Differential expression analysis was performed with DESeq2 using the experimental batch number as a covariate in order to mitigate batch effects. Transcripts with FDR below 0.1 were considered significantly differentially expressed.

Adipsin AAV versus GFP AAV differential expression analysis.—Raw demultiplexed FASTQ files were aligned to the mouse genome mm10/GRCm38 using STAR aligner version 2.5.2b[50] in mode -twopassMode Basic. Mapped reads per gene were counted using the Rsubread R package[51]. Differential expression analysis was performed using DESeq2[48] using sequencing batch as covariate. Genes with FDR below 0.1 were considered significantly differentially expressed.

Pathway analysis.—Enrichr[44,45] was utilized for pathway analyses on gene sets from WT islets treated with C3a and palmitate.

Statistical analysis.

Unless otherwise stated, data are presented as mean ± s.e.m. Data are derived from multiple experiments unless stated otherwise. No statistical method was used to calculate sample size, but sample size was determined based on preliminary experiments and previous publications. For all animal experiments, weight and fasting glucose were measured before treatments and animals were weight- and glucose-matched. Animal studies were performed without blinding of the investigator. If not mentioned otherwise in the figure legend, statistical significance is indicated by $*P < 0.05$, $**P < 0.01$ and $***P < 0.001$. Statistical

analysis was carried out using unpaired, two-tailed *t*-test or two-way ANOVA. GraphPad Prism 7 was used for statistical analysis.

Human study methods.

Study sample.—The Framingham Heart Study (FHS) is a community-based, prospective longitudinal cohort. We studied participants attending the following baseline examinations: Offspring Cohort Exam 7 (1998–2001, $n = 3,539$) and Third-Generation Cohort Exam 1 (2002–2005, $n = 4,095$)[52,53]. From this sample, we excluded individuals with end-stage kidney disease (estimated glomerular filtration rate, eGFR < 30 ml per min per 1.73 m^2), prevalent cardiovascular disease (myocardial infarction, heart failure or atrial fibrillation), those without adipsin measurements and individuals missing key clinical covariates (total number excluded, $n = 748$), leaving 6,886 individuals for cross-sectional analyses. Of participants without prevalent diabetes at baseline, 5,570 attended subsequent examinations, allowing for ascertainment of new-onset diabetes mellitus (Offspring Exam 8, 2005–2008; Third Generation Exam 2, 2008–2011). This study was approved by the Partners Institutional Review Board and all participants provided written informed consent.

Clinical, biomarker and imaging assessment.—Each participant underwent a complete physical examination, anthropometry and provided a comprehensive medical history. A physician obtained resting and seated blood pressure measurements in duplicate and reported them as a single average measurement. With each subject seated for at least 5 min at rest, blood pressure was measured in the left arm. Blood plasma samples were obtained, and immediately processed and kept at −80 °C until assayed. Plasma adipsin was assayed using a modified ELISA sandwich approach, multiplexed on a Luminex xMAP platform (Sigma-Aldrich)[54,55]. The assay had a detection range of 0.8 pg ml^{-1} to 100,000 pg ml^{-1}, with inter-assay and intra-assay coefficients of variation of 6.6% and 8.2%. Fasting glucose and insulin concentrations were assayed using fasting plasma Linco insulin (Offspring) and a Linco human insulin ELISA kit (cat. no. EZHI-14K, Third Generation). A participant undergoing treatment for hyperglycemia or with a fasting glucose of ≥126 mg dl^{-1} or a non-fasting glucose of ≥200 mg dl^{-1} was classified as having diabetes. Insulin resistance was estimated using the homeostatic model assessment for insulin resistance (HOMA-IR)[56].

Cross-sectional radiographic anatomically specific adiposity volumes were obtained from participants of the Third-Generation Framingham cohort ($n = 3,068$, 2002–2005). Abdominal subcutaneous and visceral adipose tissue volumes were measures using an eight-slice multidetector CT scanner (LightSpeed Ultra, General Electric). Mean adiposity volumes in cm^3 and Hounsfield unit attenuations were recorded as previously published[57].

Statistical analysis.—Baseline clinical characteristics were summarized by cohort. Adipsin concentrations were rank normalized due to the right-skewed distribution. We examined cross-sectional associations of circulating adipsin concentrations and cardiometabolic traits, including obesity, diabetes, insulin resistance and site-specific fat depots. Analyses were adjusted for the following clinical covariates: systolic blood pressure, anti-hypertensive drug treatment, BMI, smoking status, total and high-density lipoprotein

cholesterol. We then examined the association of baseline adipsin concentrations and future development of diabetes mellitus using multivariable logistic regression. In exploratory analyses, we formally tested whether adipsin levels might modify the effect of BMI on future diabetes by including an interaction term in the model (BMI*adipsin). All analyses were conducted using SAS version 9.4 software (SAS Institute).

Genotyping, SNP selection, human tissue expression and eQTL discovery.— Genotyping within the Framingham Heart Study participants has been described previously[58]. In brief, genome-wide genotyping was performed using the Affymetrix 500K mapping arrays and 50K supplemental Human Gene Focused arrays (Affymetrix) and the Illumina Human Exome BeadChip v.1.0 (Exome Chip; Illumina). Imputation was performed using the 1000 Genomes Project Reference Panel using MACH8. We filtered results for imputation quality ratio of >0.5 and minor allele frequency (MAF) of >1%, and a genomic locus was defined using linkage disequilibrium, $r^2 < 0.1$. A GWAS of adipsin concentrations was performed using an additive genetic model. We defined *cis* variants within 1 Mb of the adipsin gene (CFD). There were 328 SNPs in this region included in our GWAS, thus *cis* variants were deemed statistically significant at a Bonferroni-corrected *P*-value threshold of $0.05/328 = 1.5 \times 10^{-4}$. Conversely, *trans* SNPs were deemed significant at a *P*-value threshold of 5×10^{-8}. We searched top SNPs for in silico associations with eQTLs and relevant clinical phenotypes[59,60].

Reporting Summary.

Further information on research design is available in the Nature Research Reporting Summary linked to this article.

Data availability

All requests for raw and analyzed data will be reviewed to verify if the request is subject to any intellectual property or confidentiality obligations. Any data and materials that can be shared will be released via a Material Transfer Agreement. Data from Framingham Heart Study participants are publicly available at dbGap according to NIH data sharing policies (study accession no. phs000007.v29.p10).

Extended Data

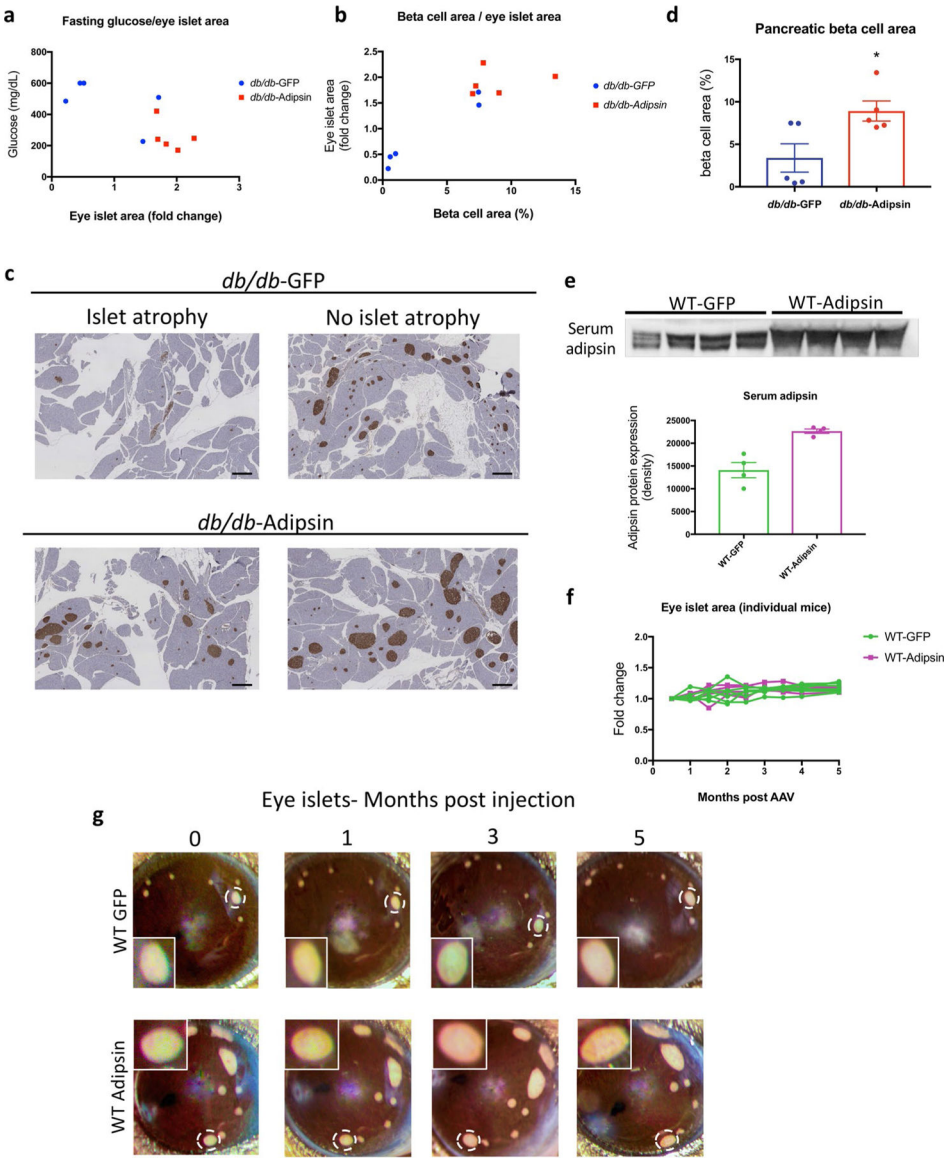

Extended Data Fig. 1 |. Islet area in the eye is correlated with beta cell area in the pancreas and lower fasting glucose.

(**a**) Scatterplot of fasting glucose levels and eye islet area in *db/db* mice transplanted with islets in the anterior chamber of the eye and treated with AAV-Adipsin or AAV GFP (n = 5 per group). (**b**) Scatterplot of beta cell area and eye islet area in *db/db* mice transplanted with islets in the anterior chamber of the eye and treated with AAV-Adipsin or AAV-GFP (n = 5 per group). (**c**) Representative immunohistochemistry images of insulin (brown) performed in pancreatic sections from *db/db*-GFP and *db/db*-Adipsin mice. IHC was performed at least twice independently with similar results. Scale bars, 100 μm. (**d**) Quantification of beta cell area in *db/db* mice transplanted with islets in the anterior chamber of the eye and treated with AAV-Adipsin or AAV-GFP (n = 5 per group). Data were analyzed by two-tailed unpaired t-test. (p = 0.027). (**e**) Western blot for adipsin from sera of B6 WT mice injected with GFP-AAV or adipsin-AAV after 5 months (n = 4 per group) along with quantification. (**f**) Quantification of islet area in the eye over time in WT-GFP and WT-Adipsin mice (n = 5

WT-Adipsin, n = 6 WT-GFP). Eye imaging was repeated at least 3 times independently with similar results. (**g**) Reporter islets transplanted into the anterior chamber of the eyes of WT-GFP and WT-Adipsin mice were serially imaged by light microscopy. Representative images are from a single mouse in each treatment group at the indicated time points. Islets are outlined within dashed white circles. Islets are amplified inside the white box. Eye imaging was repeated at least 3 times independently with similar results. Scale bars, 1 mm. Data are expressed as mean ± s.e.m. *P < 0.05, ** P < 0.01, *** P < 0.001.

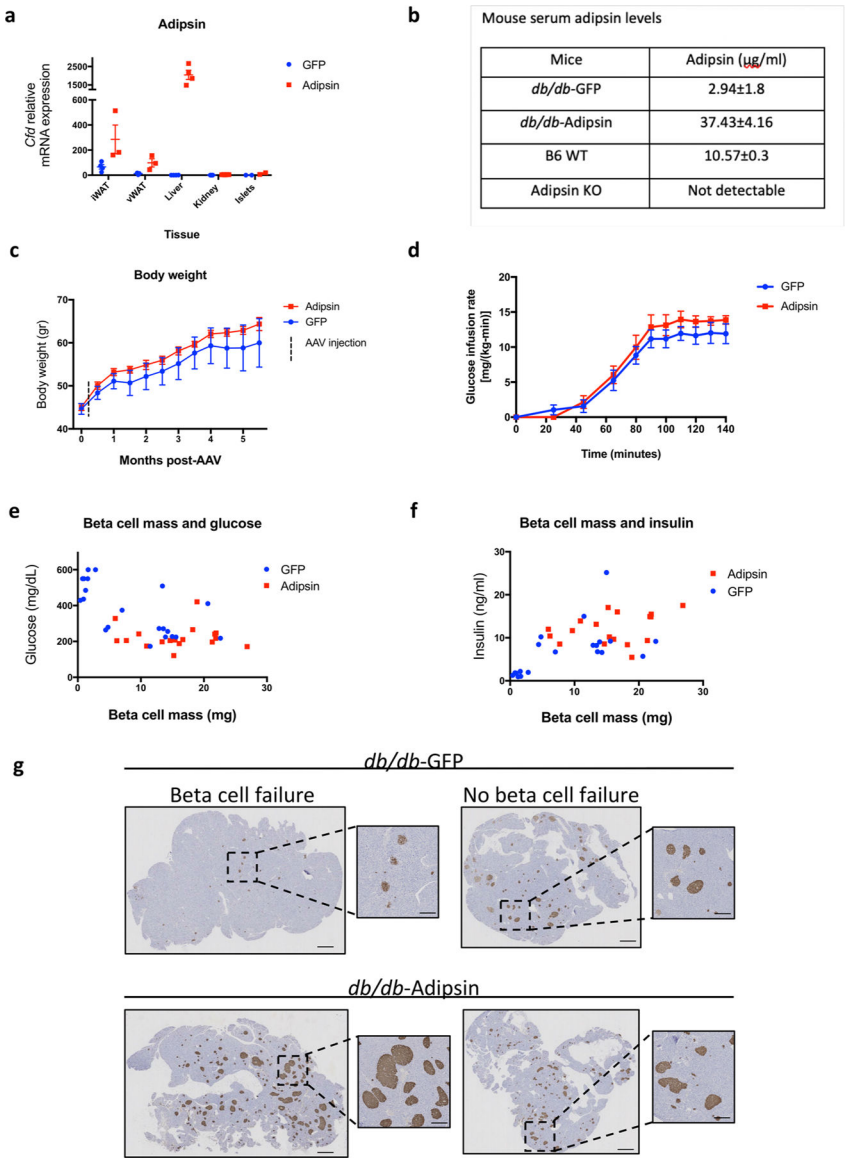

Extended Data Fig. 2 |. Treatment with AAV-Adipsin prevents beta cell failure without affecting body weight or insulin sensitivity.

(**a**) *Cfd* mRNA levels were quantified by qPCR in the indicated tissues from *db/db* mice transduced with AAV-Adipsin or AAV-GFP at 1 month post-transduction (iWAT: n = 3 *db/db*-Adipsin, n = 4 *db/db*-GFP. vWAT: n = 3 for both groups. Liver: n = 4 for both groups. Kidney: n = 6 *db/db*-Adipsin, n = 5 *db/db* GFP. Islets: n = 2 for both groups). (**b**) Mouse serum adipsin levels were measured by ELISA (n = 5 *db/db*-GFP, n = 5 *db/db*-Adipsin, n = 2 B6 WT, n = 3 Adipsin KO). (**c**) Body weights of *db/db* mice transduced with AAV-Adipsin versus AAV-GFP at the indicated time points (n = 8 mice per group at 1 month post transduction and n = 15–16 mice per group at 1.5-months post transduction). (**d**) Glucose infusion rate during hyperinsulinemic euglycemic clamp in *db/db* mice treated with adipsin versus controls (n = 5 *db/db*-Adipsin, n = 6 *db/db*-GFP). (**e**) Scatterplot of fasting glucose and beta cell mass in *db/db* mice transduced with AAV-Adipsin versus controls (n = 18–21 per group). (**f**) Scatterplot of fasting insulin and beta cell mass in *db/db* mice injected with

AAV-Adipsin versus controls (n = 18–21 per group). (**g**) Representative IHC staining for insulin (brown) in pancreases of two control and two adipsin transduced *db/db* mice. Areas in the dashed boxes are amplified in the panels at the right of each image. IHC was repeated at least twice independently with similar results. Scale bars, 1 mm left panels, 100 μm amplified regions. Data are expressed as mean ± s.e.m.

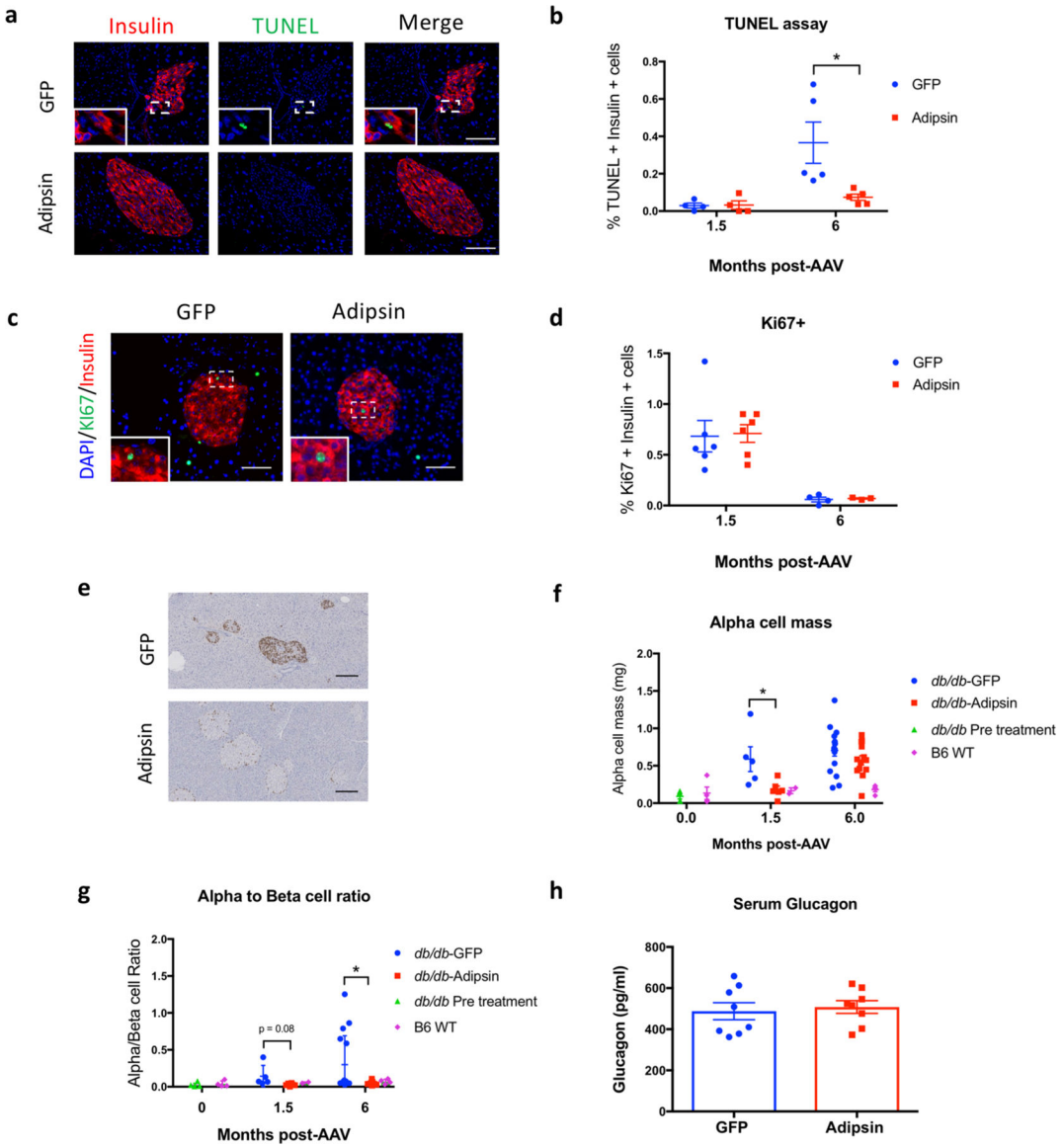

Extended Data Fig. 3 |. Adipsin prevents beta cell death and prevents loss of beta cell transcriptional identity.

(**a**) Representative images of immunofluorescence (IF) staining for insulin and TUNEL assay in pancreases of *db/db* mice injected with AAV-Adipsin versus controls. White dashed box indicates region magnified in white panel. IF was repeated at least twice independently with similar results. (**b**) Quantification of TUNEL + beta cells as determined by IF. (n = 4 mice per group at 1.5 months, n = 5 mice per group at 6 months). Data were analyzed by two-tailed unpaired t-test. (p = 0.03). (**c**) Representative images of immunofluorescence (IF) staining for insulin and Ki67 in pancreases of the indicated groups of mice. White dashed box indicates region magnified in white panel. IF was repeated at least twice independently with similar results. (**d**) Quantification of Ki67 + beta cells as determined by IF (At 1.5 months; n = 6 mice per group. At 6 months n = 3 *db/db*-Adipsin, n = 4 *db/db*-GFP). (**e**) Glucagon positive cells were quantitated by IHC in the pancreases of *db/db* mice transduced with AAV-Adipsin versus controls. Representative images are shown. IHC was repeated at

least three times independently with similar results. (**f**) Quantification of alpha cell mass in B6 WT mice, *db/db* mice treated with AAV-GFP and *db/db* mice treated with adipsin AAV at the indicated time points (Pre AAV; n = 4 *db/db*, n = 4 B6 WT. At 1.5 months post-AAV; n = 6 *db/db*-Adipsin, n = 5 *db/db*-GFP, n = 2 B6 WT. At 6 months post-AAV; n = 13 *db/db*-Adipsin, n = 16 *db/db*-GFP, n = 4 B6 WT). Data were analyzed by two-tailed unpaired t-test. (At 1.5 months post-AAV *db/db*-GFP vs *db/db*-Adipsin p = 0.03). (**g**) Quantification of the ratio between alpha cell mass and beta cell mass in pancreases from the specified groups at the indicated time points (Pre AAV; n = 4 *db/db*, n = 4 B6 WT. At 1.5 months post-AAV; n = 6 *db/db*-Adipsin, n = 5 *db/db*-GFP, n = 2 B6 WT. At 6 months post-AAV; n = 13 *db/db*-Adipsin, n = 16 *db/db*-GFP, n = 4 B6 WT). Data were analyzed by two-tailed unpaired t-test. (At 6 months post-AAV *db/db*-GFP vs *db/db*-Adipsin p = 0.029). (**h**) Fasting serum glucagon levels in *db/db* mice transduced with AAV-GFP or AAV-Adipsin (n = 8 per group). Scale bars, 100 μm (**a**, **c** and **e**). Data are expressed as mean ± s.e.m. *P < 0.05, ** P < 0.01, *** P < 0.001.

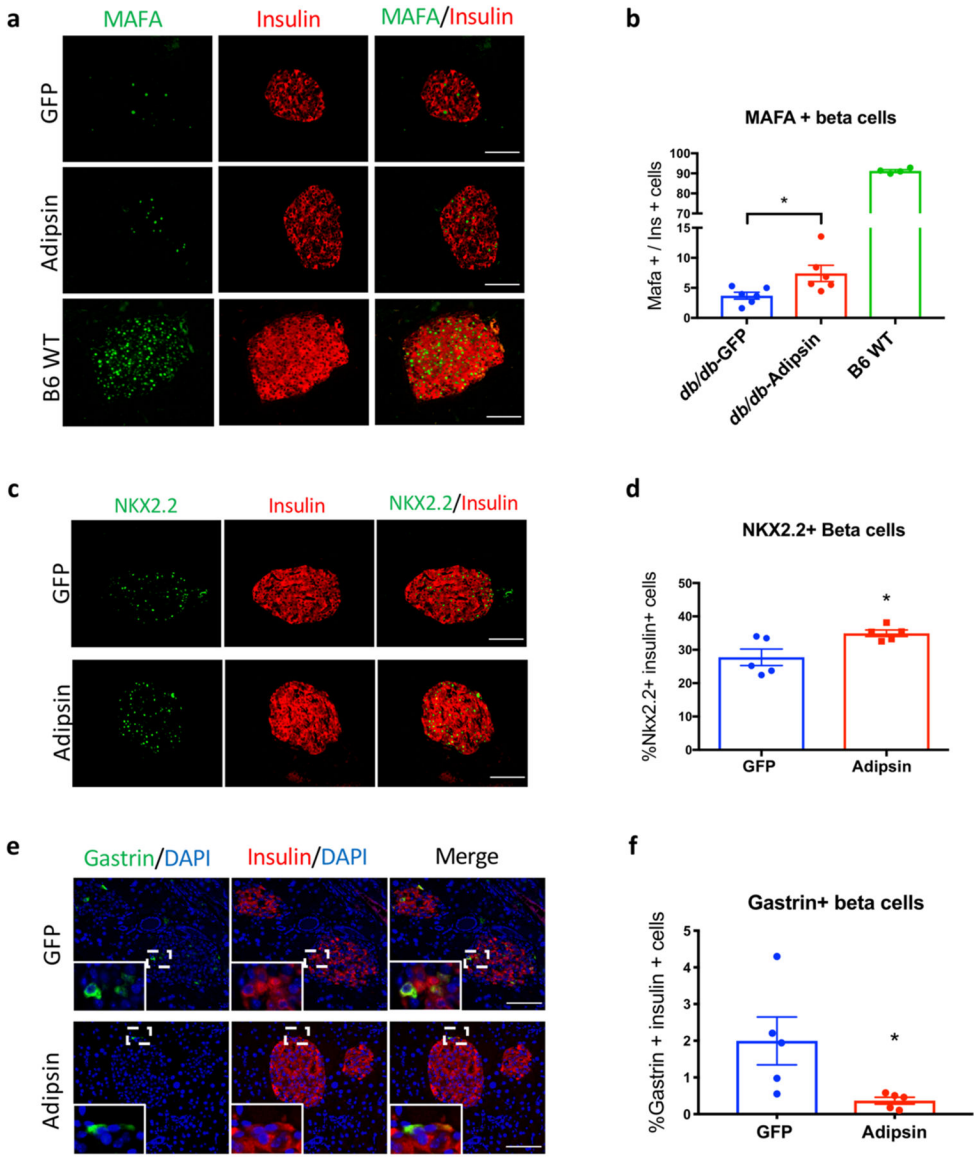

Extended Data Fig. 4 |. Adipsin increases the expression of beta cell transcription factors and decreases gastrin expression.

(**a,b**) Representative images (a) of MAFA and insulin IF in B6 WT mice, *db/db* mice injected with AAV-Adipsin or AAV-GFP along with quantification (b) of MAFA + beta cells (n = 4 mice for B6 WT, n = 6 mice per *db/db* treatment group). Data were analyzed by two-tailed unpaired t-test. (p = 0.029). (**c,d**) Representative images (c) of NKX2–2 and insulin IF in the indicated groups along with quantification (d) of NKX2–2 + beta cells (n = 5 mice per group). Data were analyzed by two-tailed unpaired t-test. (p = 0.027). (**e,f**) Representative images (e) of gastrin and insulin IF in the indicated groups along with quantification (f) of gastrin + beta cells (n = 5 mice per group). White dashed box indicates region magnified in white panel. Data were analyzed by two-tailed unpaired t-test. (p = 0.038). Scale bars, 100 μm (**a, b** and **c**). Data are expressed as mean ± s.e.m. *P < 0.05, ** P < 0.01, *** P < 0.001.

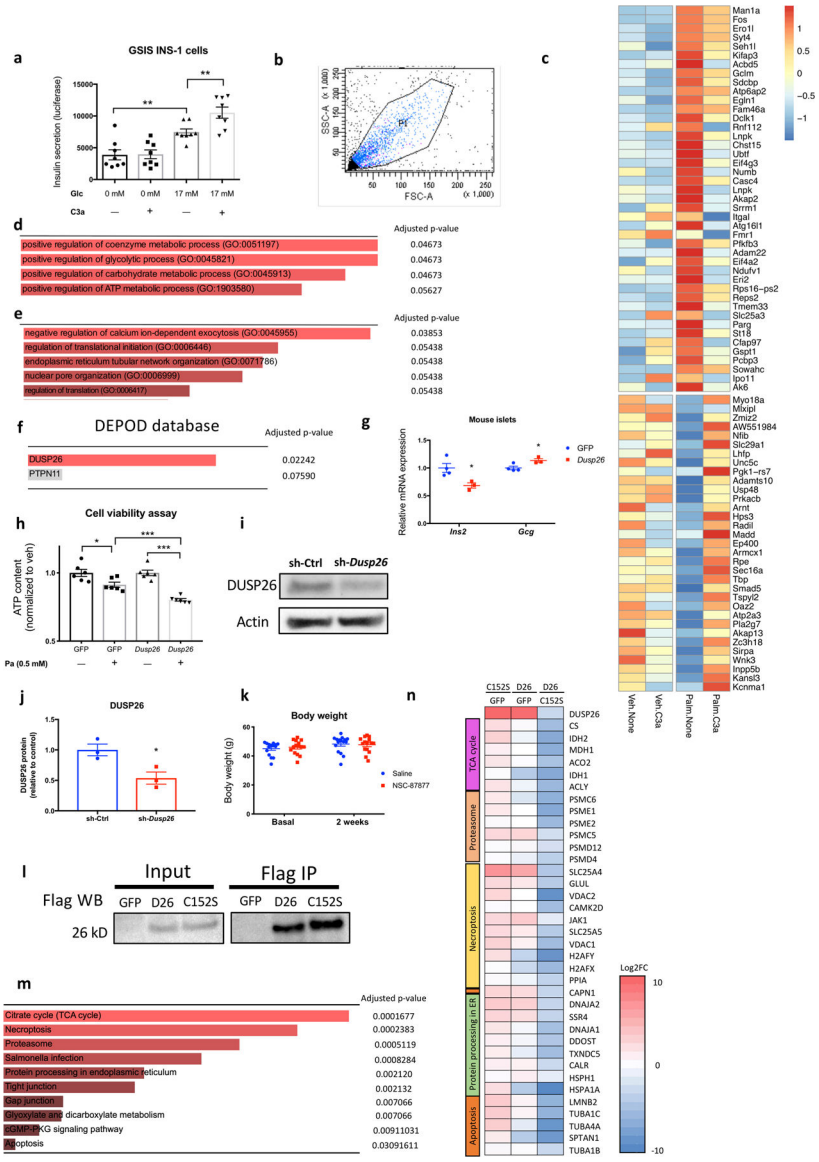

Extended Data Fig. 5 |. Adipsin/C3a increases insulin secretion and protects from beta cell death by inhibiting DuSP26.

(**a**) Ins1 beta cells were subjected to a glucose-stimulated insulin secretion assay at 0 or 17 mM glucose with or without C3a (n = 8 per group). Results are representative of three independent experiments. Data were analyzed by two-tailed unpaired t-test. (Glc 0 mM vs glc 17 mM p = 0.0019, glc 17 mM vs glc 17 mM + C3a p = 0.009). (**b**) Representative gating strategy for islet cells. (**c**) Heatmap of genes significantly changed by palmitate treatment and counter-regulated by C3a in WT islets (n = 3 per group) Colors show raw z-scores of mean normalized counts. (**d**) GO biological process analysis of genes whose expression were downregulated by palmitate and counter-regulated (increased) by C3a. Data were analyzed by Fisher/binominal test with Bonferroni-adjusted P value (n = 33 genes) (**e**) GO biological process analysis of genes whose expression were upregulated by palmitate and counter-regulated (decreased) by C3a. Data were analyzed by Fisher/binominal test with Bonferroni-adjusted P value (n = 43 genes) (**f**) Pathway analysis from the DEPOD database

depicting significant phosphatase substrates in islets that are regulated at the gene expression level by C3a from Fig. 3d. (n = 76 genes) Data were analyzed by Fisher/binominal test with Bonferroni-adjusted P value (**g**) *Ins2* and *Gcg* were determined by qPCR in isolated pancreatic islets from WT mice transduced with *Dusp26* or control lentivirus (n = 4 GFP, n = 3 *Dusp26*). Data are representative of 3 independent experiments. Data were analyzed by two-tailed unpaired t-test. (*Ins2* p = 0.0284, *Gcg* p = 0.033). (**h**) Cell viability was determined in INS-1 cells transduced with *Dusp26* and controls (n = 6 per group). Data are representative of 3 independent experiments. Data were analyzed by two-tailed unpaired t-test. (GFP in veh vs GFP in Pa p = 0.022, Dusp26 in veh vs Dusp26 in Pa p = 0.0000047, GFP in Pa vs Dusp26 in Pa p = 0.0004). (**i**) Representative western blot analysis of DUSP26 in INS-1 cells treated with shRNA against *Dusp26* versus control shRNA. Data are representative of 3 independent experiments. (**j**) Quantification of DUSP26 expression for Supplementary Figure 8d from 3 independent experiments. Data were analyzed by two-tailed unpaired t-test. (p = 0.028). (**k**) Body weight in *db/db* mice treated for 2 weeks with NSC-87877 and controls at the indicated time points (n = 15 NSC-87877 group, n = 16 saline group). (**l**) Representative western blot analysis for FLAG after immunoprecipitation of the DUSP26 protein complex using FLAG-M2 antibodies in lysates of INS-1 cells overexpressing control GFP, intact DUSP26 (D26) and catalytically inactive DUSP26 mutant (C152S). Data are representative of at least 3 independent experiments. (**m**) KEGG pathway analysis of proteins enriched in DUSP26 immunoprecipitation experiment. Proteins with log2 ≥ 1.5 between control GFP and DUSP26 mutant (C152S) were included in the analysis. Top and selected pathways are shown. Data were analyzed by Fisher/binominal test with Bonferroni-adjusted P value (n = 253 genes) (**n**) Heatmap of selected proteins belonging to relevant pathways and significantly enriched in the DUSP26 mutant (C152S) pulldown. (n = 2 per group). Colors show log2 fractional intensity. Data are expressed as mean ± s.e.m. *P < 0.05, ** P < 0.01, *** P < 0.001.

Clinical Characteristic	Offspring (n =2957)	Third Generation (n =3929)	Combined (n =6886)
Age, years	60±9	40±9	49±14
Women, n (%)	1647 (56)	2096 (53)	3743 (54)
Systolic blood pressure, mmHg	127±18	117±10	121±17
Diastolic blood pressure, mmHg	74±10	72±9	73±9
Body mass index, kg/m^2	28.0 ±5.3	26.8 ±5.5	27.3 ±5.4
Waist Circumference (cm)	99±14	93±15	96 ±15
Diabetes mellitus, n (%)	283 (10)	117 (3)	400 (6)
Hypertension treatment, n(%)	930 (31)	318 (8)	1248 (18)
Current smoking, n (%)	394 (13)	668 (17)	1062 (15)
Total Cholesterol, mg/dL	202±36	189±35	194±36
High Density Lipoprotein, mg/dL	54±17	54±16	54±17

Extended Data Fig. 6 |. Baseline participant characteristics.

The average adipsin concentration was 900 ± 273 ng/mL (mean ± s.d.) Values depict mean ± standard deviation where appropriate.

A. Cross-sectional Correlates

Clinical Traits	OR	95% CI	p
Prevalent Diabetes Mellitus	0.69	0.61 - 0.78	<0.0001
Obesity (not BMI adjusted)	1.68	1.56 - 1.80	<0.0001

	β	S.E.	p
BMI	1.34	0.06	<0.0001
Waist Circumference	0.22	0.08	0.004
Insulin	-0.02	0.01	0.12
Fasting Glucose	-0.46	0.12	<0.0001
HOMA-IR	-0.03	0.01	0.01
HOMA-β	0.01	0.01	0.29
SBP	0.17	0.20	0.38
DBP	-0.39	0.12	0.002
HDL Cholesterol	-1.15	0.19	<0.0001
Triglycerides	0.00	0.006	0.77

B. Radiographic (CT) Volumetric Measure of Adiposity

Anatomical Adipose Site	β	S.E.	P
Subcutaneous Adipose Tissue	0.04	0.01	0.0002
Visceral Adipose Tissue	0.001	0.01	0.87
Pericardial Fat	0.01	0.02	0.47
Intra Thoracic Adipose Tissue	0.03	0.01	0.03

Extended Data Fig. 7 |. Clinical correlates of adipsin.

(**a**) In cross-section multivariable analyses, higher adipsin levels associate with lower odds of diabetes (OR 0.69) and with higher odds of obesity (OR 1.68). Adipsin is associated with a number of clinical traits including BMI, waist circumference, diastolic blood pressure reduction and reduced HDL cholesterol. Additionally, higher levels associate with significantly lower fasting glucose, with a trend toward improved insulin resistance as measured by HOMA-IR that did not meet the Bonferroni-corrected p-value threshold for significance. Analyses were multivariable linear (t statistic) or logistic regression models (Wald Chi-square test) with two-sided p-values deemed significant at a Bonferroni-corrected p-value threshold of p = 0.05/10 primary traits = 0.005. Similar results were obtained in secondary analyses stratified by Framingham cohort (Offspring vs. Third Generation). (**b**) Cross-sectional radiographic anatomically specific adiposity volumes were obtained from participants of the Third-Generation Framingham cohort (n = 3068, 2002 to 2005). In

secondary analyses, volumetric measures of adiposity reveal that adipsin is strongly associated with subcutaneous (SAT) and intrathoracic adipose volumes and not visceral adipose volumes. With regard to subcutaneous adipose, a one standard deviation rise in adipsin was associated with a 0.4 standard deviation increase in subcutaneous adipose volume. Analyses were multivariable linear regression models (t statistic) with two-sided p-values deemed significant at a p-value threshold of $p = 0.05$.

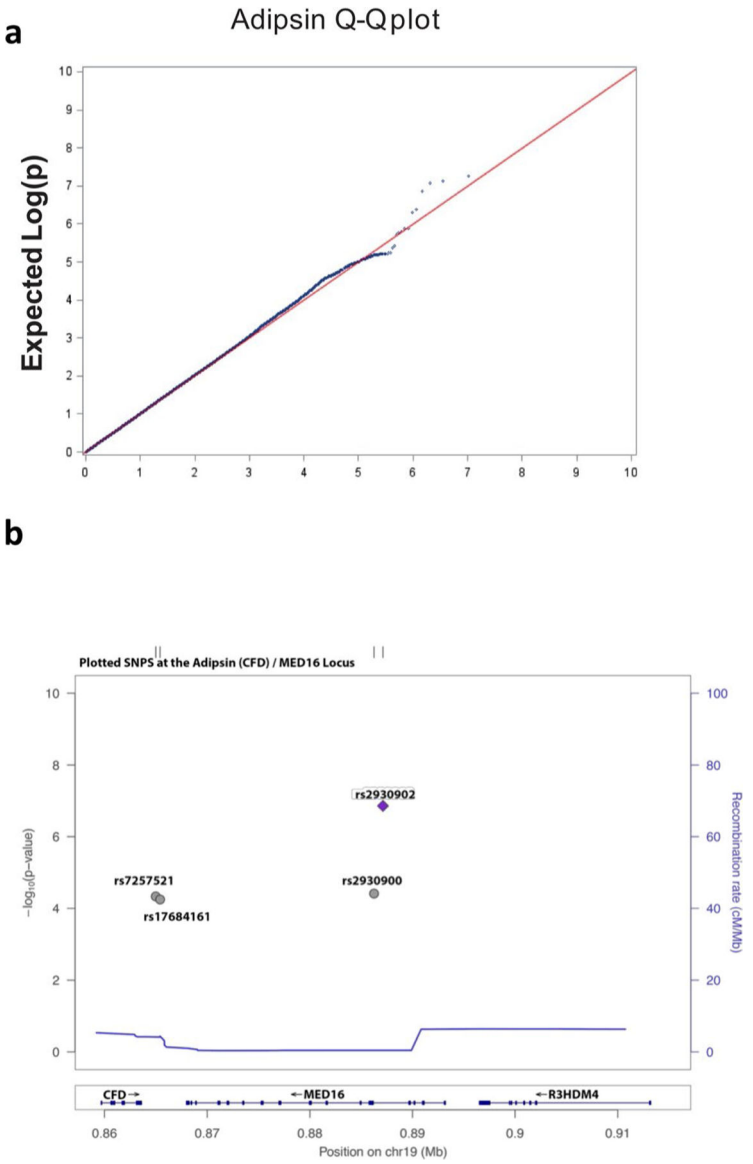

Extended Data Fig. 8 |. GWAS of adipsin levels in the Framingham Cohort.

A genome-wide association study of adipsin levels was conducted among n = 6791 individuals with available genetic data using an additive genetic model (t statistic). (**a**) A quintile-quintile plot of the observed and expected P-values. Each dot represents observed data while the solid line represents the null hypothesis of no association. (**b**) A regional plot of the sentinel SNP (rs2930902) associated with elevated plasma adipsin level is housed intronically within the MED16. Other significant cis-SNPs are also shown.

snpid	chr	location	imaf	beta	se	pval	effect	noneffect	locus	consequence / variant type	PheWAS P <0.05	cis-QTL p <0.05	metabolites, p <0.05
rs2930902	19	19:887128	0.83	0.13	0.02	1.39E-07	A	G	MED16	MED16 intron variant	**DM**, LDL cholesterol	CFD (subcut adipose, periph blood, skeletal muscle), MED16 (pancreas, subcut adipose)	Glycine, Valine, Omega-6 fatty acids
rs2930900	19	19:886257	0.78	0.11	0.03	3.79E-05	A	G	MED16	MED16 intron variant	**DM**	CFD (whole blood, hippocampus, hypothalamus, skeletal muscle, spleen); MED16 (pancreas)	Glycine, Valine
rs7257521	19	19:864992	0.88	-0.16	0.04	4.58E-05	A	G	MED16/CFD	downstream variant	**DM**	CFD (subcut adipose, skin); MED16 (heart left ventricle, liver, lung, ovary), PCSK4	x
rs17684161	19	19:865406	0.86	-0.11	0.03	5.60E-05	T	C	MED16/CFD	downstream variant	**DM**, Glomerular Filtration Rate, Atopic Dermatitis	CFD (tibial artery), PCSK4 (Heart atrial appendage), MED16 (heart left ventricle, testis, peripheral blood); FGF22 (pancreas)	hypoxanthine, phenol sulfate, mannose

Extended Data Fig. 9 |. Significant cis variant SNPs with phenotypic association, eQTL analysis, and associated metabolites from published databases.

The lead SNP on chromosome 19 rs2930902 is an intron variant in the MED16 locus and is associated with type 2 diabetes. Tissue specific cis-eQTL's reveal that this SNP is significantly associated with adipsin expression in a number of tissues but notably in subcutaneous (but not visceral) adipose tissue. Moreover, the same SNP is associated with known branch chain amino acid metabolites (glycine and valine) known to predict incident type 2 diabetes mellitus. Three additional SNPs associated with adipisin expression are shown.

Acknowledgements

N.G.-B. is supported by an American Diabetes Association postdoctoral fellowship (1-18-PMF-032). J.S.G. was supported by an MGH NIH T32 Training Grant (HL007208), the John S. LaDue Memorial Fellowship and the MGH Physician Scientist Development Program. This work was supported by a Weill Cornell Department of Medicine Seed Grant for Innovative Research to J.C.L., the JPB Foundation (to B.M.S.), Jill Roberts IBD Institute (to G.P.) and NIH grants DK097303 (to J.C.L.), R03 DK111762 (to J.C.L.), R01 DK121844 (to J.C.L.), R01 HL140224 (to J.E.H.) and R01 HL134893 (to J.E.H.). This work was partially supported by the National Heart, Lung and Blood Institute's Framingham Heart Study (contracts N01-HC-25195 and HHSN268201500001I) and by the Division of Intramural Research (to P.C., G.S., C.L., S.-J.H. and D.L.) of the National Heart, Lung and Blood Institute. We acknowledge support from the Yale Mouse Metabolic Phenotyping Center via NIH grants nos. U24 DK-059635, R01 DK116774, R01 DK114793 and P30 DK045735 (all to G.I.S.). We acknowledge the Microscopy and Image Analysis Core Facility at Weill Cornell Medicine for analysis of the images presented in this study, J. Cao for his help with confocal microscopy and the Human Islet and Adenovirus Core of the Einstein–Sinai Diabetes Research Center (NIH grant no. P30 DK020541-38) for the human islet studies. The views expressed in this Letter are those of the authors and do not necessarily represent the views of the National Institute of Diabetes and Digestive and Kidney Diseases, National Heart, Lung and Blood Institute, the National Institutes of Health or the US Department of Health and Human Services.

References

1. Alejandro EU, Gregg B, Blandino-Rosano M, Cras-Meneur C. & Bernal-Mizrachi E. Natural history of beta-cell adaptation and failure in type 2 diabetes. Mol. Aspects Med 42, 19–41 (2015). [PubMed: 25542976]
2. Rahier J, Guiot Y, Goebbels RM, Sempoux C & Henquin JC Pancreatic beta-cell mass in European subjects with type 2 diabetes. Diabetes Obes. Metab 10(Suppl. 4), 32–42 (2008). [PubMed: 18834431]
3. Turner RC, Cull CA, Frighi V & Holman RR Glycemic control with diet, sulfonylurea, metformin or insulin in patients with type 2 diabetes mellitus: progressive requirement for multiple therapies (UKPDS 49). UK Prospective Diabetes Study (UKPDS) Group. JAMA 281, 2005–2012 (1999). [PubMed: 10359389]

4. Kahn SE et al. Glycemic durability of rosiglitazone, metformin or glyburide monotherapy. N. Engl. J. Med 355, 2427–2443 (2006). [PubMed: 17145742]
5. Lo JC et al. Adipsin is an adipokine that improves beta cell function in diabetes. Cell 158, 41–53 (2014). [PubMed: 24995977]
6. DeFronzo RA et al. Type 2 diabetes mellitus. Nat. Rev. Dis. Primers 1, 15019 (2015). [PubMed: 27189025]
7. Kahn SE, Cooper ME & Del Prato S Pathophysiology and treatment of type 2 diabetes: perspectives on the past, present and future. Lancet 383, 1068–1083 (2014). [PubMed: 24315620]
8. Kasuga M Insulin resistance and pancreatic beta cell failure. J. Clin. Invest 116, 1756–1760 (2006). [PubMed: 16823472]
9. Ferrannini E The stunned beta cell: a brief history. Cell Metab. 11, 349–352 (2010). [PubMed: 20444416]
10. Ouchi N, Parker JL, Lugus JJ & Walsh K Adipokines in inflammation and metabolic disease. Nat. Rev. Immunol 11, 85–97 (2011). [PubMed: 21252989]
11. Ilegems E et al. Reporter islets in the eye reveal the plasticity of the endocrine pancreas. Proc. Natl Acad. Sci. USA 110, 20581–20586 (2013). [PubMed: 24248353]
12. Li G et al. Multifunctional in vivo imaging of pancreatic islets during diabetes development. J. Cell Sci 129, 2865–2875 (2016). [PubMed: 27270669]
13. Dalboge LS et al. Characterisation of age-dependent beta cell dynamics in the male *db*/*db* mice. PLoS One 8, e82813 (2013). [PubMed: 24324833]
14. Rosen BS et al. Adipsin and complement factor D activity: an immune-related defect in obesity. Science 244, 1483–1487 (1989). [PubMed: 2734615]
15. Gomez-Banoy N. & Lo JC. Genetic manipulation with viral vectors to assess metabolism and adipose tissue function. Methods Mol. Biol 1566, 109–124 (2017). [PubMed: 28244045]
16. Baron AD, Schaeffer L, Shragg P & Kolterman OG Role of hyperglucagonemia in maintenance of increased rates of hepatic glucose output in type II diabetics. Diabetes 36, 274–283 (1987). [PubMed: 2879757]
17. Mezza T et al. Insulin resistance alters islet morphology in nondiabetic humans. Diabetes 63, 994–1007 (2014). [PubMed: 24215793]
18. Henquin JC & Rahier J Pancreatic alpha cell mass in European subjects with type 2 diabetes. Diabetologia 54, 1720–1725 (2011). [PubMed: 21465328]
19. Talchai C, Xuan S, Lin HV, Sussel L & Accili D Pancreatic beta cell dedifferentiation as a mechanism of diabetic beta cell failure. Cell 150, 1223–1234 (2012). [PubMed: 22980982]
20. Guo S et al. Inactivation of specific beta cell transcription factors in type 2 diabetes. J. Clin. Invest 123, 3305–3316 (2013). [PubMed: 23863625]
21. Kim-Muller JY. et al. Aldehyde dehydrogenase 1a3 defines a subset of failing pancreatic beta cells in diabetic mice. Nat. Commun 7, 12631 (2016). [PubMed: 27572106]
22. Dahan T et al. Pancreatic beta-cells express the fetal islet hormone gastrin in rodent and human. Diabetes 66, 426–436 (2017). [PubMed: 27864307]
23. Sharma RB & Alonso LC Lipotoxicity in the pancreatic beta cell: not just survival and function, but proliferation as well? Curr. Diab. Rep 14, 492 (2014). [PubMed: 24740729]
24. Wang JY, Lin CH, Yang CH, Tan TH & Chen YR Biochemical and biological characterization of a neuroendocrine-associated phosphatase. J. Neurochem 98, 89–101 (2006). [PubMed: 16805799]
25. Shi Y et al. NSC-87877 inhibits DUSP26 function in neuroblastoma resulting in p53-mediated apoptosis. Cell Death Dis. 6, e1841 (2015). [PubMed: 26247726]
26. Song M et al. NSC-87877, inhibitor of SHP-1/2 PTPs, inhibits dual-specificity phosphatase 26 (DUSP26). Biochem. Biophys. Res. Commun 381, 491–495 (2009). [PubMed: 19233143]
27. Belgardt BF et al. The microRNA-200 family regulates pancreatic beta cell survival in type 2 diabetes. Nat. Med 21, 619–627 (2015). [PubMed: 25985365]
28. Prentki M & Nolan CJ Islet beta cell failure in type 2 diabetes. J. Clin. Invest 116, 1802–1812 (2006). [PubMed: 16823478]
29. Zhou Q et al. Relationship between serum adipsin and the first phase of glucose-stimulated insulin secretion in individuals with different glucose tolerance. J. Diabetes Investig 9, 1128–1134 (2018).

30. Rosen ED & Spiegelman BM What we talk about when we talk about fat. Cell 156, 20–44 (2014). [PubMed: 24439368]
31. Type 2 Diabetes Knowledge Portal rs2930902. type2diabetesgenetics.org 2019 Feb 1; http://www.type2diabetesgenetics.org/variantInfo/variantInfo/rs2930902#
32. Type 2 Diabetes Knowledge Portal rs2930900. type2diabetesgenetics.org 2019 Feb 1; http://www.type2diabetesgenetics.org/variantInfo/variantInfo/rs2930900#
33. Type 2 Diabetes Knowledge Portal rs7257521. type2diabetesgenetics.org 2019 Feb 1; http://www.type2diabetesgenetics.org/variantInfo/variantInfo/rs7257521#
34. Type 2 Diabetes Knowledge Portal rs17684161. type2diabetesgenetics.org 2019 Feb 1; http://www.type2diabetesgenetics.org/variantInfo/variantInfo/rs17684161#
35. Wang TJ et al. Metabolite profiles and the risk of developing diabetes. Nat. Med 17, 448–453 (2011). [PubMed: 21423183]
36. Kettunen J et al. Genome-wide study for circulating metabolites identifies 62 loci and reveals novel systemic effects of LPA. Nat. Commun 7, 11122 (2016). [PubMed: 27005778]
37. Ishida E, Kim-Muller, J. Y. & Accili, D. Pair feeding, but not insulin, phloridzin or rosiglitazone treatment, curtails markers of beta-cell dedifferentiation in *db*/*db* mice. Diabetes 66, 2092–2101 (2017). [PubMed: 28506962]
38. Camporez JP et al. Cellular mechanism by which estradiol protects female ovariectomized mice from high-fat diet-induced hepatic and muscle insulin resistance. Endocrinology 154, 1021–1028 (2013). [PubMed: 23364948]
39. Mellado-Gil J. et al. Disruption of hepatocyte growth factor/c-Met signaling enhances pancreatic beta-cell death and accelerates the onset of diabetes. Diabetes 60, 525–536 (2011). [PubMed: 20980460]
40. Burns SM et al. High-throughput luminescent reporter of insulin secretion for discovering regulators of pancreatic beta-cell function. Cell Metab. 21, 126–137 (2015). [PubMed: 25565210]
41. Rappsilber J, Ishihama Y & Mann M Stop and go extraction tips for matrix-assisted laser desorption/ionization, nanoelectrospray and LC/MS sample pretreatment in proteomics. Anal. Chem 75, 663–670 (2003). [PubMed: 12585499]
42. Elias JE & Gygi SP Target–decoy search strategy for increased confidence in large-scale protein identifications by mass spectrometry. Nat. Methods 4, 207–214 (2007). [PubMed: 17327847]
43. Huttlin EL et al. A tissue-specific atlas of mouse protein phosphorylation and expression. Cell 143, 1174–1189 (2010). [PubMed: 21183079]
44. Chen EY et al. Enrichr: interactive and collaborative HTML5 gene list enrichment analysis tool. BMC Bioinformatics 14, 128 (2013). [PubMed: 23586463]
45. Kuleshov MV et al. Enrichr: a comprehensive gene set enrichment analysis web server 2016 update. Nucleic Acids Res. 44, W90–W97 (2016). [PubMed: 27141961]
46. Pelossof R et al. Prediction of potent shRNAs with a sequential classification algorithm. Nat. Biotechnol 35, 350–353 (2017). [PubMed: 28263295]
47. Bray NL, Pimentel H, Melsted P & Pachter L Near-optimal probabilistic RNA-seq quantification. Nat. Biotechnol 34, 525–527 (2016). [PubMed: 27043002]
48. Love MI, Huber W & Anders S Moderated estimation of fold change and dispersion for RNA-seq data with DESeq2. Genome Biol. 15, 550 (2014). [PubMed: 25516281]
49. Soneson C, Love MI & Robinson MD Differential analyses for RNA-seq: transcript-level estimates improve gene-level inferences. F1000Res. 4, 1521 (2015). [PubMed: 26925227]
50. Dobin A et al. STAR: ultrafast universal RNA-seq aligner. Bioinformatics 29, 15–21 (2013). [PubMed: 23104886]
51. Liao Y, Smyth GK & Shi W The Subread aligner: fast, accurate and scalable read mapping by seed-and-vote. Nucleic Acids Res. 41, e108 (2013). [PubMed: 23558742]
52. Splansky GL et al. The third generation cohort of the national heart, lung and blood institute's Framingham Heart Study: design, recruitment and initial examination. Am. J. Epidemiol 165, 1328–1335 (2007). [PubMed: 17372189]

53. Kannel WB, Feinleib M, McNamara PM, Garrison RJ & Castelli WP An investigation of coronary heart disease in families. The Framingham offspring study. Am. J. Epidemiol 110, 281–290 (1979). [PubMed: 474565]

54. Carson RT & Vignali DA Simultaneous quantitation of 15 cytokines using a multiplexed flow cytometric assay. J. Immunol. Methods 227, 41–52 (1999). [PubMed: 10485253]

55. dupont NC, Wang K, Wadhwa PD, Culhane JF & Nelson EL Validation and comparison of luminex multiplex cytokine analysis kits with ELISA: determinations of a panel of nine cytokines in clinical sample culture supernatants. J. Reprod. Immunol 66, 175–191 (2005). [PubMed: 16029895]

56. Matthews DR et al. Homeostasis model assessment: insulin resistance and beta-cell function from fasting plasma glucose and insulin concentrations in man. Diabetologia 28, 412–419 (1985). [PubMed: 3899825]

57. Lee JJ et al. Cross-sectional associations of computed tomography (CT)-derived adipose tissue density and adipokines: the Framingham Heart Study. J. Am. Heart Assoc 5, e002545 (2016). [PubMed: 26927600]

58. Sotoodehnia N et al. Common variants in 22 loci are associated with QRS duration and cardiac ventricular conduction. Nat. Genet 42, 1068–1076 (2010). [PubMed: 21076409]

59. Staley JR et al. PhenoScanner: a database of human genotype–phenotype associations. Bioinformatics 32, 3207–3209 (2016). [PubMed: 27318201]

60. Consortium GT Human genomics. The Genotype-Tissue Expression (GTEx) pilot analysis: multitissue gene regulation in humans. Science 348, 648–660 (2015). [PubMed: 25954001]

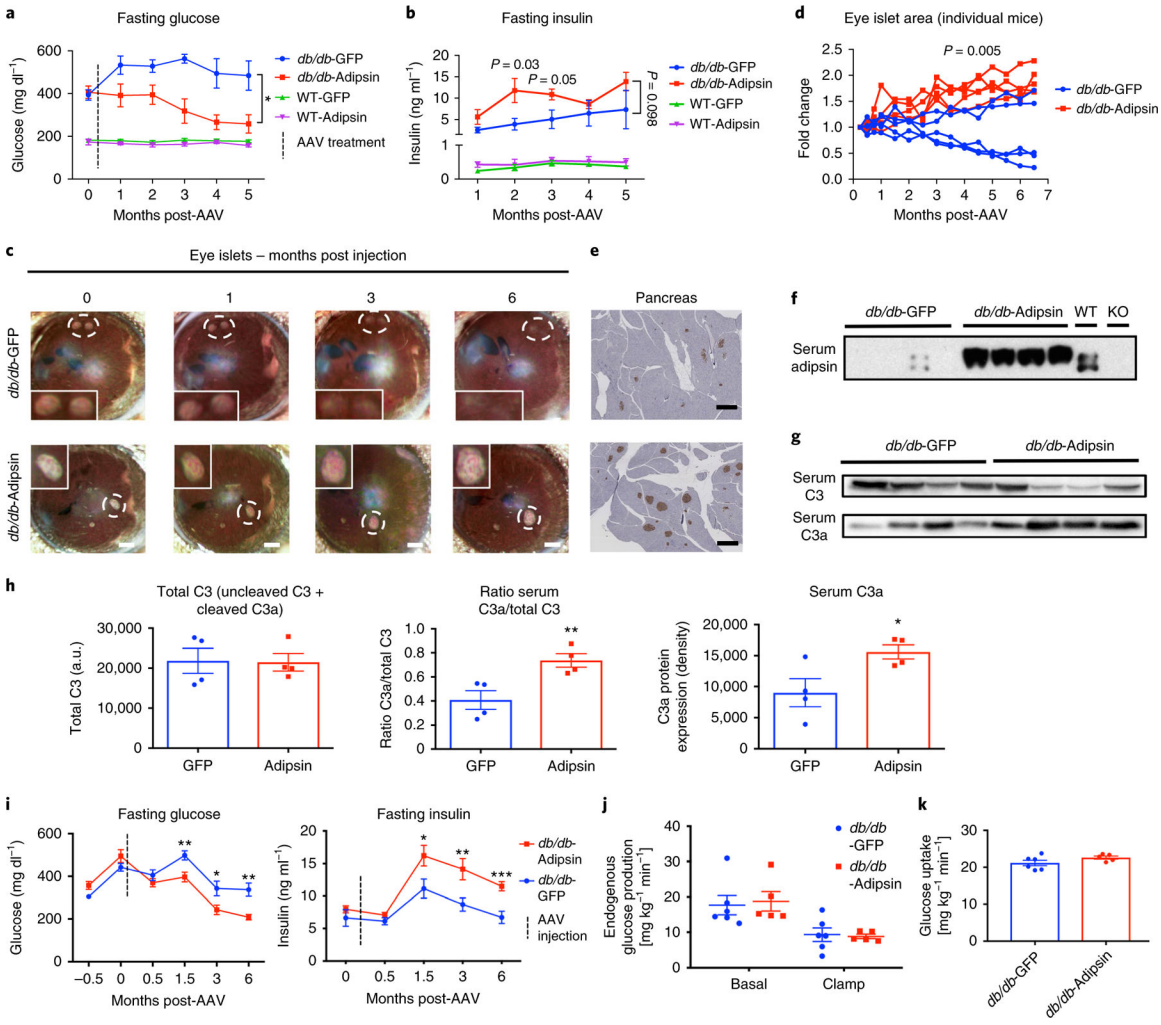

Fig. 1 |. Adipsin prevents islet atrophy and ameliorates hyperglycemia in diabetic mice.

a,**b**, Fasting glucose (**a**) and fasting insulin (**b**) levels of *db*/*db*-GFP, *db*/*db*-Adipsin, WT-GFP and WT-Adipsin at the indicated time points ($n = 5$ *db*/*db*-GFP, $n = 5$ *db*/*db*-Adipsin, $n = 6$ WT-GFP, $n = 5$ WT-Adipsin). Data were analyzed by two-way analysis of variance (ANOVA) with repeated measures and unpaired *t*-test at the indicated time points (*db*/*db*-Adipsin versus *db*/*db*-GFP $P = 0.018$ (**a**)). **c**, Reporter islets transplanted into the anterior chamber of the eyes of *db*/*db*-GFP and *db*/*db*-Adipsin mice were serially imaged by light microscopy. Representative images are from a single mouse in each treatment group at the indicated time points. Islets are outlined within dashed white circles. Islets are magnified inside the white box. Scale bars, 1 mm. Eye imaging was repeated at least three times, independently, with similar results. **d**, Quantification of islet area in the eye over time in *db*/*db*-GFP and *db*/*db*-Adipsin mice ($n = 5$ per group). Data were analyzed by two-way ANOVA with repeated measures. **e**, Representative immunohistochemistry (IHC) images of insulin (brown) performed in pancreatic sections from the same mouse as the eye islet images in **c**. Scale bars, 100 μm. IHC was performed twice, independently, with similar results. **f**, Western blot for adipsin from sera of *db*/*db* mice injected with GFP-AAV or Adipsin-AAV after 6 months. WT and adipsin knockout (KO) mice sera serve as controls.

Note: Adipsin-AAV has an epitope tag, which is why it migrates at a higher apparent molecular weight than the endogenous Adipsin. Western blot was performed at least five times in independent cohorts with similar results. **g**,**h**, Western blot (**g**) and quantification (**h**) of uncleaved C3 and C3a in the sera ($n = 4$ per group). Data were analyzed with two-tailed unpaired test. (Ratio of serum C3a/total C3 GFP versus adipsin $P = 0.0138$, serum C3a GFP versus adipsin $P = 0.0399$.) Western blots were performed at least twice in independent cohorts with similar results. **i**, Fasting glucose and fasting insulin levels in *db*/*db* mice in both treatment groups at the indicated time points (pre-AAV and 0 months (baseline): $n = 7$ *db*/*db*-Adipsin, $n = 8$ *db*/*db*-GFP; 0.5 months post-AAV: $n = 13$ db/db-Adipsin, $n = 17$ *db*/*db*-GFP; 1.5 months post-AAV: $n = 15$ *db*/*db*-Adipsin, $n = 16$ *db*/*db*-GFP; 3 and 5 months post-AAV: $n = 14$ *db*/*db*-Adipsin, $n = 17$ *db*/*db*-GFP). Data were analyzed by two-tailed unpaired *t*-test at each time point. (Glucose: 1.5 months post-AAV $P = 0.0025$, 3 months post-AAV $P = 0.027$, 6 months post-AAV $P = 0.0012$; insulin: 1.5 months post-AAV $P = 0.025$, 3 months post-AAV $P = 0.0065$, 5 months post-AAV $P = 0.0005$.) **j**,**k**, Glucose uptake rates (**j**) and endogenous glucose production (**k**) measured during a hyperinsulinemic euglycemic clamp of *db*/*db* mice transduced with adipsin or control ($n = 5$ *db*/*db*-Adipsin, $n = 6$ *db*/*db*-GFP) per group. Data are expressed as mean ± s.e.m. $*P < 0.05$, $**P < 0.01$, $***P < 0.001$.

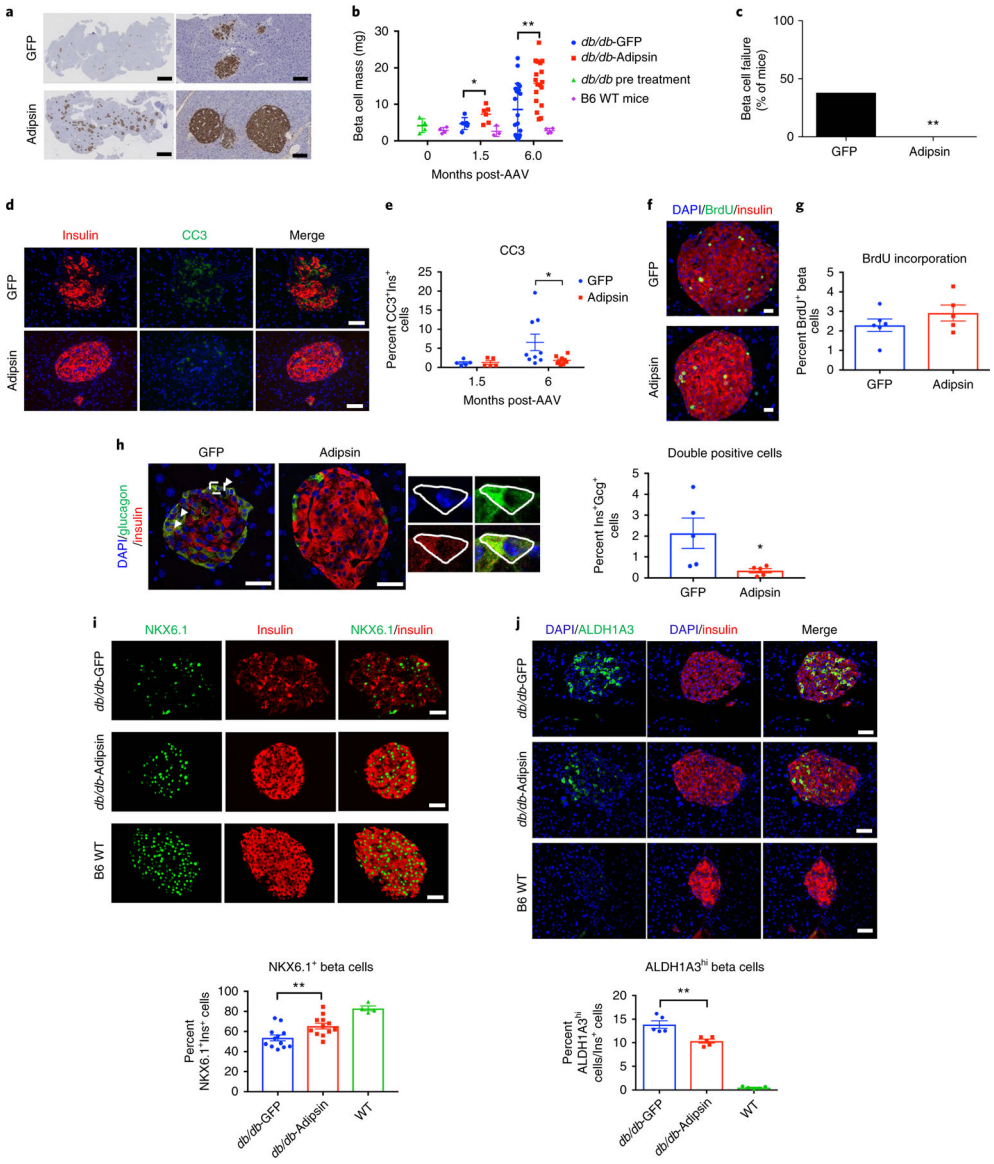

Fig. 2 |. Adipsin prevents beta cell failure in *db*/*db* mice by blocking beta cell death and dedifferentiation.

a, Representative IHC staining for insulin (brown) in pancreases of control and adipsin transduced *db*/*db* mice. Scale bars, 1 mm (left), 100 μm (right). IHC was performed at least twice, independently, with similar results. **b**, Quantification of beta cell mass in B6 WT mice, *db*/*db* mice pre AAV treatment, *db*/*db* mice treated with control or adipsin AAV at the indicated time points. Each point represents a mouse. (Pre-AAV: $n = 4$ *db*/*db*, $n = 4$ B6 WT mice; at 1.5 months post-AAV: $n = 6$ for both *db*/*db* groups, $n = 3$ B6 WT; at 6 months post-AAV: $n = 21$ *db*/*db*-GFP, $n = 18$ *db*/*db*-Adipsin, $n = 4$ B6 WT.) Data were analyzed by two-tailed unpaired *t*-test at each time point (1.5 months post-AAV $P = 0.049$, 6 months post-AAV $P = 0.0018$). **c**, Percent of control or adipsin-treated *db*/*db* mice with beta cell failure defined as severely diminished beta cell mass (<3 mg), severe hyperglycemia (>450 mg dl $^{-1}$) and profound insulinopenia (<3 ng ml^{-1}) ($n = 18$ *db*/*db*-Adipsin, 21 *db*/*db*-GFP). Data were analyzed by two-sided Fisher's exact test ($P = 0.004$). **d**, Representative images of

immunofluorescence (IF) staining for insulin and cleaved caspase 3 (CC3) in pancreases of both indicated groups of mice. IF was repeated at least twice, independently, with similar results. **e**, Quantification of $CC3^+$ beta cells as determined by IF ($n = 5$ mice per group at 1.5 months, 9 mice per group at 6 months). Data were analyzed by two-tailed unpaired *t*-test ($P = 0.047$). **f**, Representative images of IF staining for insulin and BrdU in pancreases from the indicated groups of *db*/*db* mice. IF was repeated at least twice, independently, with similar results. **g**, Quantification of $BrdU^+$ beta cells as determined by IF ($n = 6$ mice per group). **h**, Left: Representative confocal microscopy images of pancreatic islets stained for insulin (Ins) and glucagon (Gcg) in adipsin and GFP transduced *db*/*db* mice. Arrows indicate Ins^+Gcg^+ cells. The white box indicates the region magnified in the far right panels. Images are separated by channels. Outlined is an Ins^+Gcg^+ cell. Right: Quantification of Ins^+Gcg^+ cells as determined by IF in the indicated groups. Each point represents an individual mouse ($n = 5$ mice per group). Data were analyzed by two-tailed unpaired *t*-test ($P = 0.043$). **i**, Representative images of NKX6.1 and insulin IF in B6 WT mice, *db*/*db* mice treated with AAV-GFP and *db*/*db* mice treated with AAV-Adipsin along with quantification of $NKX6.1^+$ beta cells ($n = 4$ for B6 WT mice, $n = 12$ mice per *db*/*db* group). Data were analyzed by two-tailed unpaired *t*-test ($P = 0.009$). **j**, Representative images of ALDH1A3 and insulin IF in B6 WT mice, *db*/*db* treated with AAV-GFP or AAV-Adipsin and quantification of $ALDH1A3^{hi}$ beta cells ($n = 5$ per group). Data were analyzed by two-tailed unpaired *t*-test ($P = 0.0041$). Scale bars in **d**,**f**,**h**,**i**,**j**, 100 μm. Data are expressed as mean ± s.e.m. $*P < 0.05$, $**P < 0.01$, $***P < 0.001$.

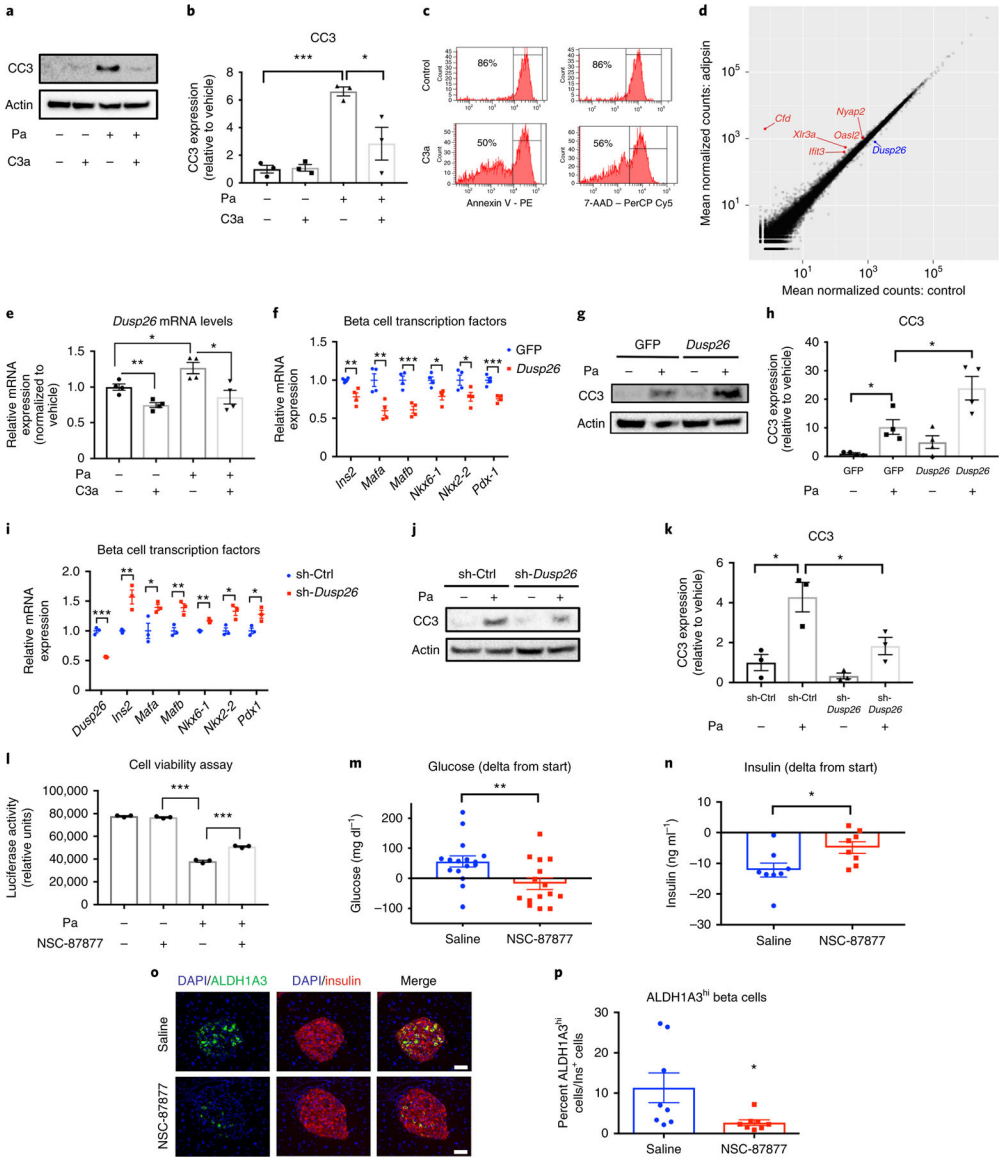

Fig. 3 |. Adipsin/C3a regulates Dusp26, a phosphatase that regulates beta cell identity and survival.

a, INS-1 beta cells were treated with vehicle (Veh) or palmitate (Pa) (0.5 mM) with or without recombinant C3a (100 nM), and CC3 expression was determined by western blot. A representative immunoblot is shown. The experiment was repeated three times, independently. **b**, Quantification of CC3 expression from three independent experiments. Data were analyzed by two-tailed unpaired *t*-test (Veh versus Pa $P = 0.0002$, Pa versus Pa + C3a $P = 0.0371$). **c**, Flow cytometry analysis for annexin V and 7-AAD in isolated islets from WT mice treated with palmitate (0.5 mM) with or without recombinant C3a. Data are representative of two independent experiments. **d**, Scatterplot of RNA–seq analyses from islets of *db*/*db* mice treated with adipsin or control AAV. Genes significantly induced by adipsin are in red and those that are downregulated in blue ($n = 3$–4 per group). **e**, *Dusp26* mRNA levels were quantified by qPCR in INS-1 cells treated in Veh or Pa conditions with or without C3a ($n = 4$ per group). Data are representative of three independent experiments.

Data were analyzed by two-tailed unpaired *t*-test (Veh versus Veh + C3a $P = 0.004$, Veh versus Pa $P = 0.026$, Pa + Pa + C3a $P = 0.017$). **f**, Beta cell identity genes in INS-1 cells transduced with Dusp26 versus control were determined by qPCR ($n = 4$ per group). Data are representative of three independent experiments. Data were analyzed by two-tailed unpaired *t*-test (*Ins2* $P = 0.007$, *Mafa* $P = 0.008$, *Mafb* $P = 0.001$, *Nkx6–1* $P = 0.016$, *Nkx2–2* $P = 0.048$, *Pdx-1* $P = 0.001$). **g**, INS-1 cells transduced with Dusp26 or control were treated with Veh or Pa and CC3 was determined by western blot. A representative immunoblot is shown. Data are representative of at least three independent experiments. **h**, Quantification of CC3 expression from three independent experiments. Data were analyzed by two-tailed unpaired *t*-test (GFP in Veh versus GFP in Pa $P = 0.011$, GFP in Pa versus *Dusp26* in Pa $P = 0.031$). **i**, qPCR analysis of beta cell identity genes in INS-1 cells treated with shRNA targeting Dusp26 versus control shRNA ($n = 3$ per group). Data are representative of three independent experiments. Data were analyzed by two-tailed unpaired *t*-test (*Dusp26* $P = 0.0002$, *Ins2* $P = 0.009$, *Mafa* $P = 0.046$, *Mafb* $P = 0.01$, *Nkx6–1* $P = 0.0015$, *Nkx2–2* $P = 0.019$, *Pdx1* $P = 0.027$). **j**, Representative western blot analysis for CC3 in INS-1 cells treated with shRNA against Dusp26 versus controls under Veh or Pa conditions. Data are representative of three independent experiments. **k**, Quantification of CC3 expression from three independent experiments. Data were analyzed by two-tailed unpaired *t*-test (sh-Ctrl in Veh versus sh-Ctrl in Pa $P = 0.017$, sh-Ctrl in Pa versus sh-*Dusp26* in Pa $P = 0.045$). **l**, Cell viability was determined in WT islets treated with Veh or Pa (0.5 mM) in the presence or absence of the DUSP26 inhibitor, NSC-87877 (20 μM; $n = 3$ per group). Data are representative of three independent experiments. Data were analyzed by two-tailed unpaired *t*-test (Veh versus Pa $P = 0.000002$, Pa versus Pa + NSC-87877 in Pa $P = 0.0002$). **m**, *db*/*db* mice were treated with NSC-87877 or saline for 2 weeks. Changes in fasting glucose levels at 2 weeks of treatment compared to basal of NSC-87877 treated mice and controls ($n = 15$ NSC-87877, $n = 16$ saline). Data were analyzed by two-tailed unpaired *t*-test ($P = 0.009$). **n**, Changes in fasting insulin levels at 2 weeks of treatment compared to basal in indicated groups ($n = 8$ per group). Data were analyzed by two-tailed unpaired *t*-test ($P = 0.026$). **o**,**p**, Representative images of ALDH1A3 and insulin IF in pancreas from NSC-87877 treated *db*/*db* mice and controls (**o**) along with quantification of ALDH1A3^{hi} beta cells (**p**) ($n = 8$ per group). Scale bars, 100 μm. Data were analyzed by two-tailed unpaired *t*-test ($P = 0.037$). Data are expressed as mean ± s.e.m. $*P < 0.05$, $**P < 0.01$, $***P < 0.001$.

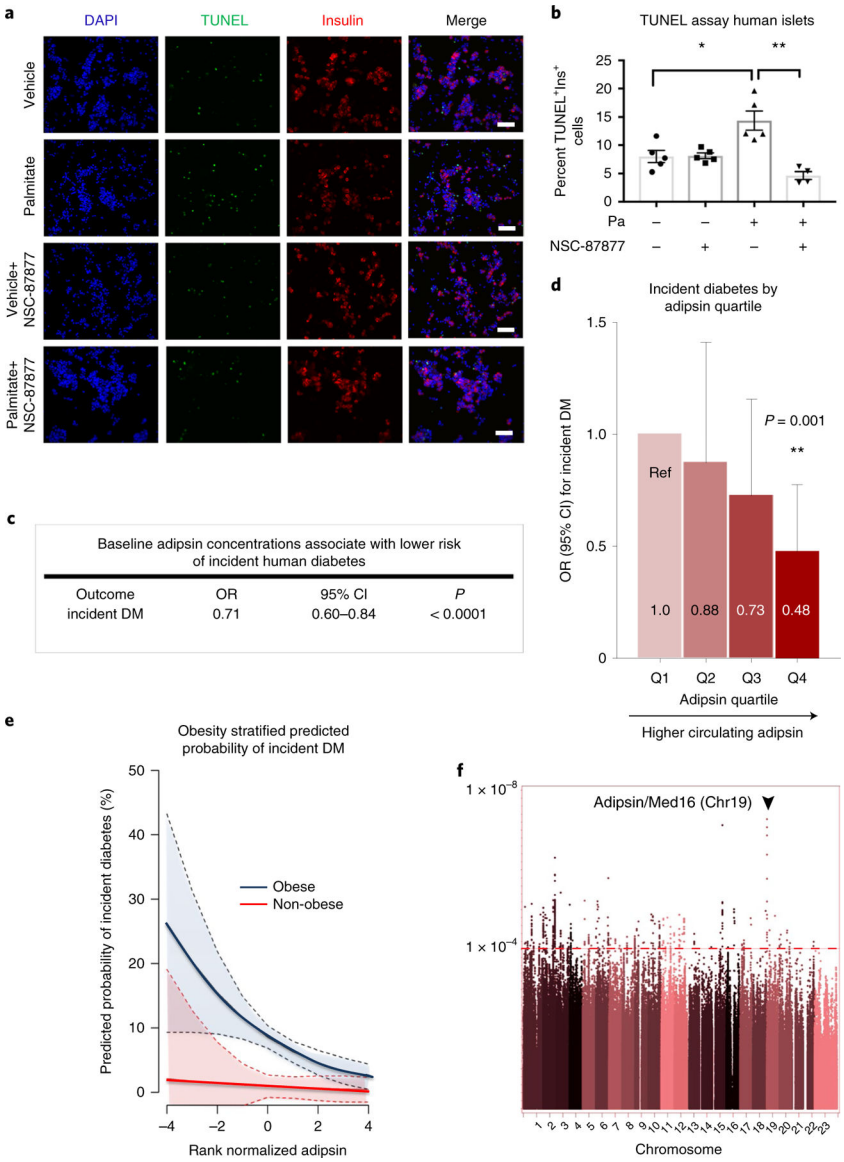

Fig. 4 |. DuSP26 inhibition protects human beta cells and circulating adipsin is associated with protection from future diabetes in humans.

a, Dispersed human islets were treated with Veh or Pa (0.5 mM) with or without NSC-87877 (20 μM). Representative images are presented of IF staining for insulin and TUNEL assay in dispersed human islets. Images are representative of two independent experiments. **b**, Quantification of TUNEL$^+$ human beta cells as determined by IF (n = 5 for Veh, Veh + NSC-87877 and Pa; n = 4 for Pa + NSC-87877 group). Data are pooled from two independent experiments. Data were analyzed by two-tailed unpaired t-test (Veh versus Pa P = 0.012, Pa versus Pa + NSC-87877 P = 0.0042). Scale bars, 100 μm. Data are expressed as mean ± s.e.m. *P < 0.05, **P < 0.01, ***P < 0.001. **c**, Ascertainment of new-onset diabetes mellitus occurred in participants without prevalent diabetes at baseline and who attended subsequent examinations (n = 5,570). When controlled for BMI, a 1 s.d. increase in adipsin is associated with a 29% decreased odds of future diabetes (DM, diabetes mellitus) using multivariable logistic regression (Wald chi-squared test). A two-sided P-value threshold of

<0.05 was deemed significant. **d**, Quartiles with higher circulating adipsin are associated with a decreased odds ratio of incident diabetes in a longitudinal cohort of 5,570 subjects without baseline diabetes in a multivariable logistic regression model (Wald chi-squared test). A two-sided *P*-value threshold of <0.05 was deemed significant. Adipsin concentrations are higher across quartiles; Q1–Q4 (mean ± s.d.) values were 611 ± 94 ng ml^{-1} (Q1, reference), 785 ± 40 ng ml^{-1} (Q2), 931 ± 49 ng ml^{-1} (Q3), 1,249 ± 233 ng ml^{-1} (Q4). **e**, Adipsin modifies the effect of obesity on future diabetes (*P* for interaction = 0.027 using a multiplicative interaction term in multivariable logistic regression (Wald chi-squared test)). A two-sided *P*-value threshold of <0.05 was deemed significant. Stratified analyses reveal that the association of higher adipsin levels with future diabetes risk is more pronounced among obese individuals (blue line) than non-obese individuals (red line), where the association is attenuated. Error bars represent 95% confidence intervals, the *x* axis scale represents rank-normalized units, with 0 representing the median and each 1 unit representing a 1 s.d. change in adipsin level. **f**, A genome-wide association study (GWAS) of adipsin levels was conducted among $n = 6{,}791$ individuals with available genetic data using a linear mixed model (asymptotic chi-squared). Genome-wide association for each single-nucleotide polymorphism (SNP) is represented in relation to the genomic position on its respective autosome. A Bonferroni-adjusted significance threshold for a *cis*-pQTL ($P < 1.5 \times 10^{-4}$) is indicated for the adipsin locus on chromosome 19. The sentinel SNP is indicated by an arrowhead.